The Journal of Chemical Physics

RESEARCH ARTICLE | MAY 02 2025

On the modeling of hydrocarbon combustion in external electric fields with reactive molecular dynamics

Navraj S. Lalli ; Andrea Giusti

Check for updates

J. Chem. Phys. 162, 174311 (2025)
https://doi.org/10.1063/5.0264365

View Online
Export Citation

Articles You May Be Interested In

Atomistic insight into the effects of electrostatic fields on hydrocarbon reaction kinetics
J. Chem. Phys. (February 2023)

Hydrogen irradiation-driven computational surface chemistry of lithium oxide and hydroxide
J. Chem. Phys. (December 2023)

Optimization of the Reax force field for the lithium–oxygen system using a high fidelity charge model
J. Chem. Phys. (August 2020)

06 May 2025 09:58:34

AIP Publishing



The Journal of Chemical Physics
Special Topics Open for Submissions
Learn More
AIP Publishing

The Journal of Chemical Physics ARTICLE pubs.aip.org/aip/jcp

On the modeling of hydrocarbon combustion in external electric fields with reactive molecular dynamics

Cite as: J. Chem. Phys. 162, 174311 (2025); doi: 10.1063/5.0264365
Submitted: 10 February 2025 • Accepted: 9 April 2025 •
Published Online: 2 May 2025

View Online Export Citation CrossMark

Navraj S. Lalli[a] and Andrea Giusti

AFFILIATIONS

Department of Mechanical Engineering, Imperial College London, South Kensington Campus, London SW7 2AZ, United Kingdom

[a]Author to whom correspondence should be addressed: nsl16@ic.ac.uk

ABSTRACT

The use of electric fields may provide a mechanism to enable fuel-flexible technologies in aviation. The development of such technologies requires methodologies able to accurately quantify electric field effects on chemical reactions at the molecular level. This work provides a comprehensive assessment of methodologies used in the framework of reactive molecular dynamics (MD) with the reactive force field ReaxFF. The focus is on the computation of atomic charges, the method used for equilibration, and the use of global thermostats for hydrocarbon combustion in an external electric field. The charge equilibration method (QEq) and the charge transfer with polarization current equilibration method (QTPIE) were analyzed for the computation of atomic charges. For the fuel–oxygen system investigated, QEq leads to molecules with a sizable spurious net charge. QTPIE leads to more accurate molecular charges but at the cost of underestimating some atomic charges. This leads to faster combustion kinetics with QEq compared with QTPIE. A two-step equilibration procedure provides a more equilibrated system compared to widely used equilibration procedures. Furthermore, using a global thermostat with an external electric field results in an artificial reduction in fuel and oxygen first-order reaction rates. These artificial effects can be avoided by not using a thermostat, but at the expense of electric-field-induced heating. Applying an external electric field without a global thermostat accelerates combustion much more with QEq compared with QTPIE, due to the larger charges predicted by QEq. This study reveals several simulation artifacts that affect reactive MD of fuel combustion and contributes toward the more accurate modeling of fuel combustion in external electric fields.

© 2025 Author(s). All article content, except where otherwise noted, is licensed under a Creative Commons Attribution (CC BY) license (https://creativecommons.org/licenses/by/4.0/). https://doi.org/10.1063/5.0264365

06 May 2025 09:58:34

I. INTRODUCTION

Transportation is responsible for around 15% of global greenhouse gas emissions each year.[1] A substantial portion of these emissions, 11% in 2018, is from aviation, and it was estimated that aviation has contributed to 4% of human-induced global warming (as of 2021).[2] Electrification is a viable approach for reducing emissions from land transport, particularly as the amount of electricity generated from renewables continues to increase.[3] Aviation is more difficult to electrify, however, because the energy density of state-of-the-art batteries is insufficient, at present, to allow for fully electric long-distance flights.[4] Alternative approaches are, therefore, being considered to reduce the environmental impact of aviation, including the use of alternative fuels and energy carriers, such as hydrogen and sustainable aviation fuels (SAFs). The development of alternative fuels is challenging because the resulting fuel must have similar properties to conventional jet fuels such as Jet A and Jet A-1 to allow for their use in current combustion technologies. This limits which alternative fuels are appropriate for aviation and also limits the use of approved SAFs to blends with conventional jet fuels where the SAF component is typically less than 50% by weight.[5,6] Nevertheless, SAFs provide a viable way for reducing emissions from aviation. Another promising solution is hybrid thermal–electric propulsion,[7] which could also benefit from the use of SAFs.

It has recently been proposed that electric fields, created from the electrical energy necessarily available on an aircraft powered by

© Author(s) 2025

hybrid thermal–electric propulsion, could be used to increase the fuel flexibility of existing engines used in aviation,[8–10] i.e., to enable these engines to operate efficiently using fuels with a wider range of properties. For example, the fuel could be injected in the form of a charged fuel spray and an electric field used to dictate where the fuel vapor is released, which could provide an element of control over fuel–air mixing and pollutant emissions. In addition, electric fields may affect combustion through the polarization of molecules and the force exerted on ions that form during the combustion process;[11] however, further research is needed to better understand the effects of electric fields on combustion chemistry at the molecular level.

Reactive molecular dynamics (MD) with the popular reactive force field ReaxFF[12] allows the combustions of SAF constituents, such as linear or branched hydrocarbons, to be simulated at the molecular level at a relatively low cost, at least compared to quantum mechanics simulations. In addition, an electric field can be incorporated into the simulations, allowing the effects of electric fields on chemical kinetics to be explored. Numerous studies have employed ReaxFF to simulate fuel combustion, with[13–22] and without[23–32] external electric fields. The simulation approach is, therefore, well established; however, a few parts of the reactive MD methodology for studying the combustion of fuels in external electric fields are often overlooked and deserve further attention, as is discussed next.

Since the chemical environment of each atom can change with time in reactive MD, a method is needed to compute the partial charge of each atom in the system based on its local environment. ReaxFF is usually parameterized for a specific reacting system, such as hydrocarbon combustion, with charges updated at every time step using the electronegativity equalization method (EEM).[33] The charge equilibration method (QEq)[34] is very similar, and we opt to use the nomenclature QEq here instead of EEM, in line with the nomenclature used in the popular MD code Large-scale Atomic/Molecular Massively Parallel Simulator (LAMMPS).[35] Implicit in the QEq method is the assumption that the system is a perfect conductor;[36] QEq, therefore, allows charge to transfer between non-bonded atoms irrespective of the distance between the atoms, an issue we refer to as long-range charge transfer. This can cause QEq to predict unphysical charges, leading to, for example, molecules with a sizable net charge. Even though the limitations of QEq are well known,[36,37] the effect of unphysical charges arising with QEq on reactions predicted with ReaxFF is rarely analyzed or discussed. In addition, the method commonly used to incorporate an external electric field into QEq[38,39] appears to worsen long-range charge transfer and lead to highly unphysical charges.[36] Further work is needed to understand whether alternative methods can lead to more accurate partial atomic charges at a similar computational cost, with and without an external electric field, and how the computed charges affect reaction kinetics. The charge transfer with polarization current equilibration method (QTPIE)[40] is of particular interest since it can effectively reduce long-range charge transfer.[17,19]

Another area that deserves further attention is equilibration. Starting reactive production runs from a non-equilibrium system impacts initial chemical kinetics.[41] Ideally, the fuel–oxygen system should be equilibrated at the target temperature for the productions runs, which is typically between 1500 and 2500 K,[30] and without any reactions having occurred. The key challenge with equilibration in reactive MD is that the time available for equilibration is limited by reactions. It is common practice to switch C–O and H–O bonds off during equilibration of hydrocarbon–oxygen systems to prevent reactions;[17,19,23,24,26] however, the equilibration time is still limited by the breakdown of molecules due to thermal decomposition. Most studies then either equilibrate their systems at lower temperatures than the target temperature and begin the production runs by scaling atomic velocities upward to reach the target temperature[13,14,17,19,21,24,28,29,31,32] or equilibrate their systems for very short periods of time at the target temperature,[26,27] both with the aim of preventing thermal decomposition. The first approach is problematic in that the resulting system is not equilibrated at the target temperature once the atomic velocities are scaled, while the latter approach is unlikely to provide enough time for equilibration. Another approach is needed that can better equilibrate fuel–oxygen systems under the constraints imposed by thermal decomposition.

Reactive simulations with ReaxFF are widely performed in the canonical ensemble with thermostatting performed using global thermostats[23,26] (global in the sense that the thermostat acts uniformly on all atoms, usually by applying the same velocity scaling factor to all atoms), such as the Berendsen and Nosé–Hoover (NH) thermostats. It is common practice to apply an external electric field in reactive MD while using these same global thermostats: Refs. 13, 14, and 22 use the Berendsen thermostat and Refs. 15–21 use the NH thermostat. However, global thermostats typically dissipate energy introduced into the system by the electric field too quickly,[42] and it is unclear how this affects reaction kinetics. Even without an external electric field, global thermostats artificially redistribute kinetic energy absorbed/released during chemical reactions around the system, resulting in artificial changes in reactions.[41,43] Further research is needed to understand if global thermostats can faithfully be used with external electric fields in reactive MD.

The aim of this study is to provide insights into the computation of partial atomic charges, the process used for equilibration, and the use of global thermostats in reactive MD of hydrocarbon combustion in external electric fields. The specific objectives of this work are as follows: (i) investigate if QEq can provide accurate charges, with and without an external electric field; (ii) explore if QTPIE provides a more accurate alternative to QEq; (iii) evaluate the impact of the computed charges on reaction kinetics; (iv) develop a more robust method for equilibration; and (v) analyze the effect of global thermostatting on reactions when an electric field is applied. The hydrocarbon 2,2,4,6,6-pentamethylheptane (commonly referred to as isododecane, but henceforth referred to as pentamethylheptane) was chosen for this investigation, as branched hydrocarbons constitute a significant component of many SAFs[5] and pentamethylheptane is abundant in SAFs created by the alcohol-to-jet pathway.[44,45]

The remainder of this paper is structured as follows: first, the equations governing QEq and QTPIE, including the implementation of an external electric field, are described. Following this, the reactive MD methodology used to simulate and analyze the combustion of pentamethylheptane in an external electric field is provided. The simulation results are then presented and discussed, starting with an analysis of QEq and QTPIE on three molecular systems

06 May 2025 09:58:34

© Author(s) 2025

ranging in complexity from a single pentamethylheptane molecule to pentamethylheptane in oxygen under stoichiometric conditions. A two-step equilibration procedure is then evaluated, and the effects of atomic partial charges and global thermostatting on the combustion of pentamethylheptane in an external electric field are analyzed. Conclusions close this paper.

II. METHODS

This section begins by detailing how charges are computed with QEq and QTPIE and how an electric field can be incorporated into these methods. The reactive MD simulation protocol is then described.

A. Charge computation

The electrostatic energy of a molecular system composed of N atoms when expanded up to second order in the partial charges of the atoms, q_i, is[34,46]

$$U_{\mathrm{el}} = \sum_{i=1}^{N} \left(\chi_i q_i + \eta_i q_i^2\right) + \sum_{i=1}^{N-1} \sum_{j=i+1}^{N} q_i q_j J_{ij}, \tag{1}$$

where χ_i and η_i are the absolute electronegativity (also referred to as the Mulliken electronegativity) and absolute hardness of the ith atom,[47] respectively, and J_{ij} is the Coulombic interaction between the partial charges centered on atoms i and j. Atomic partial charges are computed with QEq (and EEM) by minimizing the electrostatic energy given by Eq. (1) under the constraint

$$\sum_{i=1}^{N} q_i = q_{\mathrm{net}}, \tag{2}$$

where q_{net} is the net charge of the system.

In this study, Coulombic interactions are modeled using a shielded Coulomb potential that is widely used with ReaxFF,[23]

$$J_{ij} = \begin{cases} \dfrac{\mathrm{Tap}(r_{ij})}{4\pi\varepsilon_0}\left(r_{ij}^3 + (\gamma_i\gamma_j)^{-\frac{3}{2}}\right)^{-\frac{1}{3}}, & r_{ij} < r_{\mathrm{nonb}}, \\ 0, & \text{otherwise}, \end{cases} \tag{3}$$

where r_{ij} is the interatomic distance between atoms i and j, r_{nonb} is the non-bonded cutoff radius beyond which van der Waals and Coulombic interactions are neglected, Tap is a taper function used to prevent energy and force discontinuities when atoms cross the non-bonded cutoff radius, γ_i is the Coulomb shielding parameter of the ith atom, and ε_0 is the electric permittivity of free space. The method of computing atomic partial charges by minimizing the electrostatic energy of Eq. (1) with Coulombic interactions modeled using Eq. (3) is referred to as QEq in this study, although we appreciate that EEM is perhaps a more suitable name given that Slater orbitals are not used for Coulombic interactions and an iterative approach is not used for hydrogen atoms in this study.[34]

To demonstrate that QEq allows charge to transfer between non-bonded atoms irrespective of the distance between the atoms, consider the charges predicted by QEq for a neutral system ($q_{\mathrm{net}} = 0$) composed of two atoms ($N = 2$) separated by an infinite distance,

$$q_1 = \frac{\chi_2 - \chi_1}{2(\eta_1 + \eta_2)} \quad \text{and} \quad q_2 = -q_1. \tag{4}$$

QEq predicts that these two atoms have non-zero charges when $\chi_1 \neq \chi_2$, i.e., QEq allows charge to transfer between these infinitely separated atoms. This long-range charge transfer can lead to unphysical charges for the non-perfectly conducting fuel–oxygen systems of interest to the present study.[36]

Various methods have been proposed to overcome the shortcomings of QEq, such as QTPIE[40] and atom-condensed Kohn–Sham density functional theory (DFT) approximated to second order (ACKS2).[37] QTPIE was selected for further investigation because recent studies have shown that QTPIE can effectively reduce long-range charge transfer in fuel–oxygen systems[17,19] and since QTPIE can be implemented in MD codes using solvers written for QEq.[48] It should be added that ACKS2 is expected to provide more accurate charges than QEq and QTPIE, but at a higher computational cost.[36]

With QTPIE, the atomic partial charges are found by minimizing the electrostatic energy of Eq. (1) but after replacing the absolute electronegativity of each atom, χ, with effective electronegativities given by[48]

$$\tilde{\chi}_i = \frac{\sum_{j=1}^{N} (\chi_i - \chi_j) S_{ij}}{\sum_{m=1}^{N} S_{im}} \qquad \text{for} \quad i = 1, 2, 3, \ldots, N, \tag{5}$$

where S_{ij} is a function that decays with the interatomic distance between atoms i and j. QTPIE employs S_{ij} to penalize long-range charge transfer.

All simulations in this study were performed using LAMMPS.[35] As part of this study, QTPIE was reimplemented into LAMMPS from the original work of Kritikos and Giusti[17] and extended in functionality as a new *fix* named `fix qtpie/reaxff`, which is now available for public use. Some of the implementation details of this fix are discussed in Appendix A.

B. Charge computation with an external electric field

When modeling each atom with a single point partial charge centered at its nucleus, external electric fields are commonly applied in MD by adding a force to each atom given by[42]

$$\boldsymbol{F}_i = q_i \boldsymbol{E} \qquad \text{for} \quad i = 1, 2, 3, \ldots, N, \tag{6}$$

where $\boldsymbol{E}$ is the external electric field. This study is confined to static external electric fields. In addition, the time variation of the electric field due to atomic charges is assumed to be sufficiently small that magnetic field effects can be neglected.

The external electric field must be incorporated into the method being used to compute atomic partial charges to account for electric polarization. This may be done using the electric potential due to the static external electric field, which at the position of atom i is[49]

$$\phi_i = -\int_{\mathscr{O}}^{\boldsymbol{r}_i} \boldsymbol{E}(\boldsymbol{r}') \cdot \mathrm{d}\boldsymbol{r}', \tag{7}$$

where $\mathscr{O}$ is the position chosen as the point of 0 electric potential and $\boldsymbol{r}_i$ is the position of atom i. While ϕ_i and ϕ_j depend on $\mathscr{O}$, the difference in electric potential

$$\phi_i - \phi_j = \int_{\boldsymbol{r}_i}^{\boldsymbol{r}_j} \boldsymbol{E}(\boldsymbol{r}') \cdot \mathrm{d}\boldsymbol{r}' \tag{8}$$

does not.

06 May 2025 09:58:34

© Author(s) 2025

Several authors have incorporated an electric field into QEq by replacing the absolute electronegativities in Eq. (1), χ_i, with effective electronegativities given by[36,39,50]

$$\chi_{ai} = \chi_i + \phi_i \qquad \text{for} \quad i = 1, 2, 3, \ldots, N. \tag{9}$$

This is equivalent to adding the energy $\sum_{i=1}^{N} q_i\phi_i$ to the electrostatic energy of Eq. (1). Since the external electric field is related to the electric potential through $\boldsymbol{E} = -\nabla\phi$, the gradient of this energy is consistent with the force in Eq. (6). The subscript "a" in Eq. (9) serves as a reminder that χ_{ai} depends on the *absolute* position of the ith atom, i.e., the position relative to $\mathcal{O}$ (the origin of the MD system was used as $\mathcal{O}$ in this study). This is particularly clear when we evaluate the electric potential in Eq. (7) for a uniform electric field: $\phi_i = -\boldsymbol{r}_i \cdot \boldsymbol{E}$. Henceforth, the method of computing charges with χ_a is referred to as QEqA.

An electric field can be incorporated into QTPIE by either modifying the absolute electronegativities, χ_i, or the effective electronegativities $\tilde{\chi}_i$.[38] Since QTPIE uses differences in absolute electronegativities, we use a formulation involving electric potential differences.[51] This involves replacing the absolute electronegativities in Eq. (1), χ_i, with the effective electronegativities

$$\tilde{\chi}_{ri} = \frac{\sum_{j=1}^{N} (\chi_i - \chi_j + \beta(\phi_i - \phi_j))S_{ij}}{\sum_{m=1}^{N} S_{im}} \qquad \text{for} \quad i = 1, 2, 3, \ldots, N, \tag{10}$$

where β is a scaling factor. A subscript "r" is added to this effective electronegativity to signify that $\tilde{\chi}_{ri}$ depends on the position of atom i *relative* to nearby atoms, rather than on the absolute position of atom i. For example, the electric potential difference $\phi_i - \phi_j$ for a uniform electric field is

$$\phi_i - \phi_j = (\boldsymbol{r}_j - \boldsymbol{r}_i) \cdot \boldsymbol{E}. \tag{11}$$

The formulation used in QEqA [Eq. (9)] leads to difficulties in imposing periodic boundaries in the direction of an external electric field and has also been shown to exacerbate the long-range charge transfer issues that arise with QEq.[36] It, therefore, may be more accurate to incorporate an external electric field into QEq by replacing the absolute electronegativities in Eq. (1), χ_i, with effective electronegativities given by

$$\chi_{ri} = \chi_i + \frac{\sum_{j=1}^{N} \beta(\phi_i - \phi_j)S_{ij}}{\sum_{m=1}^{N} S_{im}} \qquad \text{for} \quad i = 1, 2, 3, \ldots, N. \tag{12}$$

The subscript "r" is used once again to indicate that this formulation depends on the position of atom i *relative* to nearby atoms. Henceforth, the method of computing charges with χ_r is referred to as QEqR. QEqR was implemented in LAMMPS in line with the implementation of `fix qtpie/reaxff` (see Appendix A) and is now available for public use as `fix qeq/rel/reaxff`.

The electric field implementation in QTPIE [Eq. (10)] and QEqR [Eq. (12)] is based on physical intuition and is advantageous in that it allows for periodic boundaries to be applied in the direction of an external electric field,[21] as discussed further in Sec. III A. It should be highlighted, however, that this implementation does not add the energy $\sum_{i=1}^{N} q_i\phi_i$ to the electrostatic energy of Eq. (1) and is, therefore, not consistent with the electric force in Eq. (6). It is still worth investigating the use of QTPIE and QEqR with the electric force of Eq. (6), as QTPIE and QEqR are expected to lead to more accurate dynamics than QEqA when considering the shortcomings of using QEqA for non-conducting systems. Furthermore, we have included a scaling factor β in the equations for $\tilde{\chi}_{ri}$ and χ_{ri}. This scaling factor should be optimized when ReaxFF is parameterized to increase the accuracy of electric polarization effects captured by these methods. We use $\beta = 1$ in this study, in alignment with Refs. 17, 19, 21, and 51, although larger values may be more accurate, as discussed later in Sec. III B.

C. Reactive molecular dynamics

All MD simulations were performed with a constant number of atoms, a constant system volume, and either a constant system temperature (NVT-MD) or a constant system energy (NVE-MD). It should be highlighted that the NVE-MD simulations were performed by integrating the equations of motion as is, such that the system energy only remains constant in the absence of an applied electric field. Two global thermostats were investigated in the NVT-MD simulations: the Nosé–Hoover (NH) thermostat[52,53] and the canonical sampling through velocity rescaling (CSVR) thermostat.[54] The NH thermostat was chosen due to its widespread use in MD, while the CSVR thermostat was chosen since it performs well and for this reason is rising in popularity.[42,55,56] Although the Berendsen thermostat is widely used in reactive MD simulations performed with ReaxFF, it was not investigated following the recommendation made by Braun *et al.*[56]

All MD simulations were performed by integrating the equations of motion with the velocity-Verlet algorithm and a time step of 0.1 fs, as recommended in Refs. 23 and 29 for high temperature reactive MD simulations. The CHO-2016 ReaxFF[26] developed for hydrocarbon combustion and pyrolysis was used throughout. A rectangular Cartesian coordinate system with basis $\{\boldsymbol{e}_x, \boldsymbol{e}_y, \boldsymbol{e}_z\}$ and coordinates $\{x, y, z\}$ is used in this study. All simulations were performed using cubic domains and with periodic boundaries in all directions, except where otherwise noted, and any simulations featuring an external electric field were subject to a static and uniform electric field in the positive z-direction of strength E_z. It is common practice to apply stronger electric fields than can be realized in practice in non-equilibrium MD due to the limited timescales that can be simulated (of the order of nanoseconds).[42] Most simulations were conducted with $E_z = 0.05$ V/Å since English and Waldron[42] identify 0.05 V/Å as a reasonable upper bound for external electric fields in molecular simulations.

Charges were updated at every time step using one of QEq, QEqA, QEqR, or QTPIE. In particular, charges were computed with the conjugate gradient method until the norm of the relative residual $<10^{-10}$,[36,57] neutral systems were considered ($q_{net} = 0$), and the nonbonded cutoff radius, r_{nonb}, was set to 10 Å.[23,26] All charges reported in this study are given as a multiple of the elementary charge, e. Simulations invoking QTPIE use the same ReaxFF as was parameterized with QEq and with Gaussian orbital exponents (see Appendix A) for each atom type taken from Ref. 38. This was done merely to avoid the arduous task of parameterizing ReaxFF,[58] although we stress that the correct approach is to reparameterize ReaxFF using QTPIE to compute charges, with the Gaussian orbital exponents and the scaling factor β as free parameters that are optimized during the parameterization procedure.

06 May 2025 09:58:34

© Author(s) 2025

For the simulations conducted to investigate the combustion of pentamethylheptane, the initial system configuration was prepared using Packmol[59] by randomly positioning 30 molecules of pentamethylheptane with a stoichiometric amount of oxygen (555 O_2 molecules) in a cubic domain with side dimensions of length 57.48 Å, chosen to achieve the target density of 200 kg/m^3. Following this, the system was minimized without an electric field applied. Equilibration was then performed, also without an electric field applied and with the C–O and H–O bond parameters set to 0.0 in the ReaxFF file to prevent oxidation.[23] At the start of equilibration, atom velocities were randomly sampled from a Gaussian distribution corresponding to 1500 K and the system was advanced using NVT-MD for 0.1 ns. For both the NH and CSVR thermostats, the thermostat temperature damping parameter was set to 50 fs. The atomic velocities were then scaled to reach the target temperature of 2000 K, and the system was equilibrated for a further 10 ps. This two-step equilibration procedure is analyzed in Sec. IV. For each case investigated in this work, ten independent simulations were conducted, aligning with different initial velocities, to improve the statistics of the obtained results. If thermal decomposition occurred during equilibration, the simulation was discarded and another was run starting from a different set of initial velocities. After equilibration, production runs were performed for 2.5 ns. For the NVT-MD production runs, the thermostat temperature damping parameter was increased to 200 fs for both the NH and CSVR thermostats. In addition, the NVE-MD production runs were started from the equilibrated systems created with the NH thermostat. During the production runs, the species information was saved every 20 fs (using `fix reaxff/species`) and snapshots of the atomic charges, positions, velocities, and image flags were saved every 100 fs.

The data files, input scripts, and force fields required to reproduce the results presented in this study are available in https://doi.org/10.5281/zenodo.15222653.

1. Species analysis

During post-processing, a bond-order cutoff of 0.3 was used to identify bonds and, therefore, molecules. First-order rate constants were computed for the consumption of pentamethylheptane and oxygen. This was done by integrating the differential equation governing first-order kinetics to obtain[28]

$$\ln \mathcal{N}_0 - \ln \mathcal{N}_t = k(t - t_0), \tag{13}$$

where $\mathcal{N}_0$ and $\mathcal{N}_t$ are the number of fuel or oxygen molecules at times t_0 and t, respectively, and k is the first-order rate constant for the fuel or oxygen. Fitting a straight line to a plot of $\ln \mathcal{N}_0 - \ln \mathcal{N}_t$ vs $t - t_0$ provides the first-order rate constant for a given species. We used $t_0 = 0$ in this study.

2. Kinetic energy analysis

The equipartition theorem states that every degree of freedom present in the Hamiltonian as a quadratic term will have an average energy of $(1/2)k_BT$, where k_B is the Boltzmann constant and T is the temperature, once the system reaches thermal equilibrium; therefore, the system's energy will be equally distributed (or equipartitioned) over these degrees of freedom.[60] The temperature of a subset of the degrees of freedom of the system can be found from the corresponding kinetic energy through

$$T_i = \frac{2K_i}{k_B n_i}, \tag{14}$$

where T_i, K_i, and n_i are the temperature, kinetic energy, and number of degrees of freedom of the subset of the system denoted by i. According to the equipartition theorem, the temperature computed should be independent of the subset of the system considered. For example, the translational, rotational, and vibrational temperatures (henceforth denoted by T_{tr}, T_{rot}, and T_{vib}, respectively), computed from the translational, rotational, and vibrational kinetic energies of the oxygen molecules, for example, in a fuel–oxygen system or of all species in the system should be equal, on average, and also equal to the system temperature.[41,61] Note that the equipartition theorem applies to vibrational degrees of freedom because of the high temperatures investigated for fuel combustion in this study.[62] Appendix B details how the translational, rotational, and vibrational kinetic energies were computed in this study.

III. ANALYSIS OF METHODS FOR CHARGE COMPUTATION

This section first presents the charges computed with QEq (including QEqA and QEqR) and QTPIE for a simple molecular system to provide insights into the properties and performance of these methods. Following this, the electric dipole moment of a single pentamethylheptane molecule subject to an electric field is analyzed. This section finishes by evaluating the performance of these methods for the fuel–oxygen system of interest to the present study.

A. Analysis I: Water and carbon dioxide in an electric field

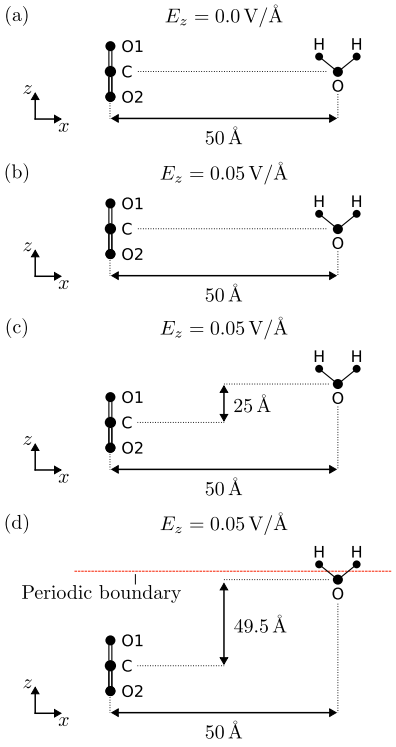
In this analysis, a water molecule (with bond length r_{OH} = 0.9572 Å and angle $\angle_{HOH}$ = 104.52°[63]) was placed 5 nm away in the x-direction from a carbon dioxide molecule (with bond length r_{CO} = 1.1621 Å and angle $\angle_{OCO}$ = 180.0°[64]), which is beyond the non-bonded cutoff radius of 1 nm, in a cubic domain with sides of length 10 nm. Both molecules were placed in the x–z plane with the oxygen atom in the water molecule placed at varying z-positions relative to the carbon atom in the carbon dioxide molecule, Δz, as illustrated in Fig. 1. With Δz = 49.5 Å, the two hydrogen atoms in the water molecule cross the top periodic boundary of the domain. The charges computed with QEq and QTPIE with and without an external electric field are shown in Fig. 1.

First, it is evident from Fig. 1(a) that the net charge of the water and carbon dioxide molecules is fractional with both QEq and QTPIE, when both molecules should be net neutral. Even if the distance between the molecules in the x-direction is increased from 5 nm to an infinite distance, these same charges are obtained. QTPIE can reduce long-range charge transfer, resulting in smaller magnitudes for the net charge of each molecule (around 50% smaller) compared with QEq, but not eliminate long-range charge transfer entirely. QTPIE achieves this by predicting a smaller magnitude for the charge of each atom in the system relative to QEq. Meanwhile, ACKS2 correctly predicts that each molecule is neutral, as it is inherent in ACKS2 that charge cannot transfer between atoms separated by a distance larger than a cutoff distance.[65]

Once an electric field is applied in the positive z-direction [see Fig. 1(b)], all methods predict that $q_{O1} > q_{O2}$ and that the

06 May 2025 09:58:34

© Author(s) 2025



All charges are given as a multiple of the elementary charge, e

Method	q_{O1}	q_C	q_{O2}	q_H	q_O	q_{mol}
QEq	-0.4930	0.8982	-0.4930	0.3407	-0.5937	**0.0877**
QTPIE	-0.4217	0.7962	-0.4217	0.2750	-0.5027	**0.0473**

Method	q_{O1}	q_C	q_{O2}	q_H	q_O	q_{mol}
QEqA	-0.4864	0.8982	-0.5002	0.3438	-0.5993	**0.0884**
QEqR	-0.4895	0.8981	-0.4962	0.3431	-0.5986	**0.0876**
QTPIE	-0.4183	0.7961	-0.4250	0.2774	-0.5076	**0.0471**

Method	q_{O1}	q_C	q_{O2}	q_H	q_O	q_{mol}
QEqA	-0.5176	0.9055	-0.5314	0.3577	-0.5718	**0.1435**
QEqR	-0.4895	0.8981	-0.4962	0.3431	-0.5986	**0.0876**
QTPIE	-0.4183	0.7961	-0.4250	0.2774	-0.5076	**0.0471**

Method	q_{O1}	q_C	q_{O2}	q_H	q_O	q_{mol}
QEqA(w)	-0.4855	0.8980	-0.4994	-0.1554	0.3976	**0.0868**
QEqA(u)	-0.5481	0.9125	-0.5619	0.3712	-0.5449	**0.1975**
QEqR	-0.4895	0.8981	-0.4962	0.3431	-0.5986	**0.0876**
QTPIE	-0.4183	0.7961	-0.4250	0.2774	-0.5076	**0.0471**

FIG. 1. A diagram illustrating the charges computed by QEq and QTPIE for each atom in a carbon dioxide and a water molecule in four scenarios: $E_z = 0.0$ V/Å in (a) and $E_z = 0.05$ V/Å in (b)–(d). In the tables, q_{mol} is the magnitude of the net charge of each molecule. In (d), QEqA(w) and QEqA(u) are the charges computed using wrapped and unwrapped coordinates, respectively.

electric dipole moment of the water molecule increases, which is the expected behavior. The effect of electric polarization is larger with QEqA compared with QEqR because the electric field affects the effective electronegativities χ_a more than the effective electronegativities χ_r.

Figure 1(c) reveals that shifting the water molecule in the positive z-direction significantly increases long-range charge transfer with QEqA: q_{mol} increases from 0.088e to 0.14e. This occurs because χ_a depends on absolute atomic positions; in particular, there is a reduction in χ_a for the atoms of the water molecule when the water molecule is displaced in the positive z-direction. This highlights how the formulation used in QEqA can exacerbate long-range charge transfer. Meanwhile, the charges predicted by QEqR and QTPIE are independent of the z-position of the water molecule, which is the expected behavior. This is because χ_r (used in QEqR) and $\tilde{\chi}_r$ (used in QTPIE) are independent of the absolute positions of the atoms.

The water molecule in Fig. 1(d) straddles the top periodic boundary. Ambiguity then arises with QEqA due to the dependence of χ_a on absolute atomic positions: there is a choice between wrapped coordinates (the atomic positions after the atoms are wrapped around the periodic boundaries) and unwrapped coordinates (the atomic positions if the periodic boundaries were not present). With wrapped coordinates [QEqA(w) in Fig. 1(d)], the partial charges on the hydrogen and oxygen atoms in the water molecule have the wrong sign. This occurs because with wrapped coordinates, the hydrogen atoms experience a much larger electric potential than the oxygen atom of the water molecule, which causes the effective electronegativity χ_a to be larger for the hydrogen atoms compared to the oxygen atom. With unwrapped coordinates [QEqA(u) in Fig. 1(d)], all partial charges have the correct sign; however, the net charge of the water molecule increases further to 0.20e. Consequently, both approaches with QEqA yield inaccurate charges when using periodic boundaries in the direction of an external electric field. In contrast, QEqR and QTPIE yield the same charges for each atom regardless of whether the water molecule is straddling a periodic boundary. This is because the implementation of QEqR and QTPIE in LAMMPS uses ghost atoms[35] across periodic boundaries when computing the absolute electronegativity differences $\chi_i - \chi_j$ and the electric potential differences $\phi_i - \phi_j$ present in Eqs. (10) and (12). As a result, QEqR and QTPIE can be used with periodic boundaries in the direction of an external electric field.

Appendix C analyzes the trajectories of two water molecules in an electric field. This simple example highlights how long-range charge transfer inherent in the QEq method can lead to unphysical trajectories when an electric field is applied and that the electric field can trigger/worsen long-range charge transfer when implemented through QEqA.

B. Analysis II: Dipole moment of a pentamethylheptane molecule

To understand the size of electric polarization effects predicted by QEqA, QEqR, and QTPIE, electric fields of varying strengths were applied to a single pentamethylheptane molecule, and the resulting electric dipole moment was computed. This was done by first minimizing a single pentamethylheptane molecule with charges computed using QEq and no electric field applied. This minimized

06 May 2025 09:58:34

© Author(s) 2025

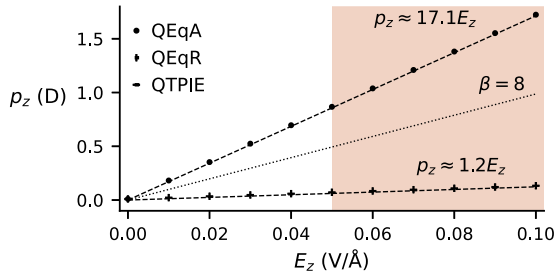


FIG. 2. The z-component of the electric dipole moment, p_z, of a pentamethylheptane molecule oriented so that the main chain is approximately in the z-direction for applied electric fields in the z-direction of strength E_z. The dipole moments are given in units of Debye (D), and the dashed lines are linear lines of best fit with the intercept discarded. The red shaded region indicates applied electric fields beyond the upper bound suggested by English and Waldron for molecular simulations.[42]

molecule was then oriented so that the sixth carbon atom in the main chain was vertically above the second carbon atom in the main chain in the z-direction.

Figure 2 presents the z-component of the electric dipole moment of the pentamethylheptane molecule. QEqA predicts a much stronger dependence of the electric dipole moment on the electric field ($p_z \approx 17.1E_z$) compared with QEqR and QTPIE ($p_z \approx 1.2E_z$). Following the analysis in Sec. III A and Appendix C, it is expected that QEqA overestimates the dipole moment of the pentamethylheptane molecule by amplifying long-range charge transfer. In addition, it is likely that QEqR and QTPIE underestimate the dipole moment, which is supported by the DFT results presented in Refs. 19 and 21 for a dodecane molecule. It may, therefore, be more appropriate to use a larger value than 1 for the scaling factor β in Eqs. (10) and (12). To provide an example, the line of best fit for QEqR and QTPIE with $\beta = 8$ is plotted in Fig. 2. Preferably, the value of β should be optimized during ReaxFF training.

C. Analysis III: Pentamethylheptane in oxygen

This analysis evaluates the charges of the pentamethylheptane and oxygen molecules in the system prepared for the combustion simulations, as detailed in Sec. II C (30 pentamethylheptane molecules, 555 oxygen molecules, 200 kg/m^3 target density). Periodic boundaries were used in the x- and y-directions, while reflecting boundaries were used in the z-direction to avoid issues with QEqA. After minimizing the system, NVT-MD simulations were performed at 1500 K using the NH thermostat. The simulations were advanced for 0.25 ns without an electric field applied and then for a further 0.25 ns with an electric field of strength $E_z = 0.05$ V/Å applied.

Figures 3(a) and 3(c) present the net charge and z-position of the pentamethylheptane molecules averaged over all pentamethylheptane molecules at each time. Figures 3(b) and 3(d) present the same quantities for the oxygen molecules. Figures 3(a) and 3(b) show that QEq leads to significant long-range charge transfer in the absence of an external electric field: the average net charge of pentamethylheptane molecules averaged over time is $1.11 \pm 0.02e$ (± standard deviation), while the corresponding net charge for the oxygen molecules is $-0.060 \pm 0.001e$. These charges are significantly smaller with QTPIE at $0.049 \pm 0.004e$ and $-0.0027 \pm 0.0002e$. QTPIE can, therefore, effectively reduce long-range charge transfer, and it achieves this by using much smaller effective electronegativities than the absolute electronegativities used in QEq, as shown in Fig. 18 of Appendix D. The charge of $0.049e$ is still expected to be much larger than any charge changes due to electric polarization. For example, atomic partial charges in a dodecane molecule changed by around $0.002e$, at most, in a very strong electric field of strength 0.1 V/Å.[19] Therefore, long-range charge transfer with both QEq and QTPIE makes it difficult to assess the influence of electric polarization on reaction kinetics. In addition, it cannot be concluded that QTPIE is more accurate than QEq on the sole basis that QTPIE predicts almost neutral molecules since a method could satisfy this criterion by predicting 0 charges for all atoms. Further analysis is provided later in this section.

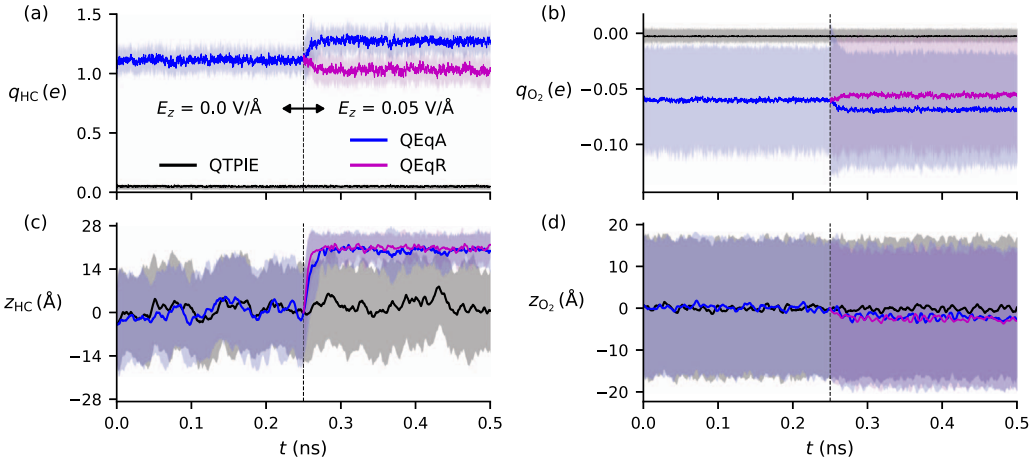


FIG. 3. The average net charge and z-position of the center of mass of (a) and (c) the pentamethylheptane molecules and (b) and (d) the oxygen molecules, before and after an electric field is applied at $t = 0.25$ ns, with QEqA, QEqR, and QTPIE. The solid lines show the average over all molecules at each time, and the shaded regions indicate the standard deviation over all molecules.

06 May 2025 09:58:34

© Author(s) 2025

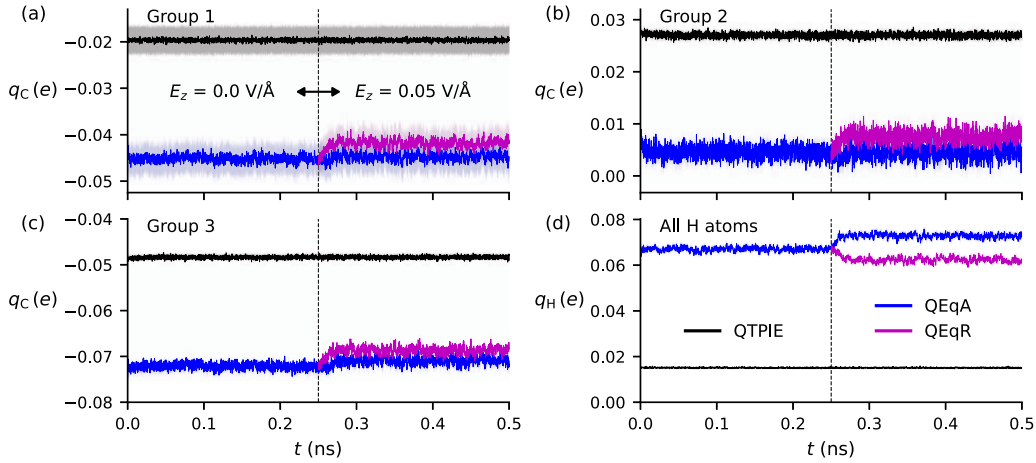


FIG. 4. (a)–(c) The average charge of carbon atoms in three carbon groups and (d) the average charge of all hydrogen atoms, before and after an electric field is applied at t = 0.25 ns, with QEqA, QEqR, and QTPIE. The solid lines show the average over all atoms in the group at each time, and the shaded regions indicate the 90% confidence interval for the average charges, which were computed using the normal distribution.

Once an electric field is applied in the z-direction (from t = 0.25 ns), it is evident from Figs. 3(c) and 3(d) that with QEqA and QEqR, the hydrocarbon molecules rise (move in the positive z-direction) in the domain due to their net positive charge, while the oxygen molecules fall in the domain due to their net negative charge. In contrast, there is no significant variation in the z-position of the hydrocarbon and oxygen molecules with QTPIE over the 0.25 ns period for which the electric field is applied. Nevertheless, over much longer periods of time, some translation in the z-direction would be expected with QTPIE since it does not eliminate long-range charge transfer entirely. Figures 3(a) and 3(b) show that long-range charge transfer is exacerbated with QEqA, but not with QEqR, as was also found in Sec. III A and Appendix C. This, once again, occurs because the effective electronegativities used by QEqA (χ_a) depend on absolute atomic positions, while those used by QEqR (χ_r) do not. For example, Fig. 18 of Appendix D shows that there is a large reduction in χ_a of the carbon and hydrogen atoms when the electric field is applied, while there are no significant changes in the χ_r values. The magnitude of the net charges of the pentamethylheptane and oxygen molecules actually fall with QEqR once the electric field is applied, which we anticipate is because of the increased repulsion between molecules (the positively charged hydrocarbon molecules are mostly in the upper half of the domain leaving less space for the negatively charged oxygen molecules to occupy). QEqA is not investigated further in this study due to its poor performance.

It is also necessary to evaluate the charges predicted by each method for each atom in the pentamethylheptane molecules. This was done by grouping the carbon atoms into groups of atoms with similar charges, which resulted in three groups. Group 1 consists of the third, fourth, and fifth carbon atoms in the main chain of seven carbon atoms in each pentamethylheptane molecule; group 2 consists of the second and sixth carbon atoms in the main chain, which are each bonded to four other carbon atoms; and group 3 consists of all other carbon atoms, which are the carbon atoms bonded to only one other carbon atom. All hydrogen atoms had reasonably similar charges so that there was no need to separate the charges into individual groups. The results of this charge analysis are presented in Fig. 4.

The time averages of the charges presented in Fig. 4 are reported in Table I for no external electric field. Table I also reports

TABLE I. Time averages of the charges predicted by QEq and QTPIE in the absence of an applied electric field and charges from the literature for carbon and hydrogen atoms in similar chemical environments. The symbol "· · ·" is used where it is unclear what value a method predicts, and [ ] is used to denote a closed interval.

Method	q_C (e)—group 1	q_C (e)—group 2	q_C (e)—group 3	q_H (e)
QEq	−0.045 ± 0.003	0.005 ± 0.001	−0.072 ± 0.001	0.067 ± 0.004
QTPIE	−0.020 ± 0.003	0.027 ± 0.001	−0.048 ± 0.001	0.015 ± 0.001
OPLS-AA[66]	[−0.12, −0.06]	0.00	−0.18	0.06
L-OPLS[67]	−0.148	0.00	−0.222	[0.074, 0.160]
PEOE[a,68]	· · ·	· · ·	−0.068	0.023
CHARGE2[b,68]	· · ·	· · ·	−0.110	0.037

[a]From the charges computed for an ethane molecule.
[b]From the charges computed for an ethane molecule.

06 May 2025 09:58:34

© Author(s) 2025

the charges for carbon and hydrogen atoms in similar chemical environments used by force fields and computed by methods in the literature for comparison. First, QEq predicts charges in reasonable agreement with the charges reported in Table I from the literature[66–68] for all four groups. However, given that QEq results in spurious net charges of size 1.11*e*, on average, for the pentamethylheptane molecules, it is expected that some of the carbon and hydrogen charges are too positive with QEq. The carbon atoms in group 2 are expected to be neutral since they are each bonded to four other carbon atoms. Both QEq and QTPIE lead to positive charges for the atoms in group 2, with QTPIE leading to more positive and, therefore, less accurate charges than QEq for group 2. For all groups except group 2, which is the group containing the fewest atoms, the charges computed with QTPIE are smaller than those computed with QEq by magnitude: the ratio of charges computed with QTPIE to the charges computed with QEq is 44% for group 1, 67% for group 3, and 22% for the hydrogen atoms. Compared to the values taken from the literature, it appears that QTPIE underestimates the magnitude of charges for all groups except group 2. This suggests that QTPIE can effectively reduce, but not eliminate, long-range charge transfer at the cost of underestimating partial atomic charges. Overall, for the fuel–oxygen system investigated, QTPIE performs well at reducing long-range charge transfer, leading to more accurate molecular charges than QEq, but achieves this by slightly underestimating the atomic charges in the pentamethylheptane molecules. It should be added that the accuracy of QTPIE is system dependent; therefore, QTPIE should be analyzed on the system of interest before deciding whether it provides sufficient accuracy.

IV. EQUILIBRATION OF A FUEL–OXYGEN SYSTEM

As discussed in the Introduction, most studies employ one of two methods to equilibrate fuel–oxygen systems under the constraints imposed by thermal decomposition. For brevity, we refer to the method that involves equilibration at a lower temperature than the target temperature as method A and the method that involves equilibration for short periods of time at the target temperature as method B. In the remainder of this section, we propose and evaluate a two-step equilibration procedure that seeks to improve upon these two methods.

In this study, the target temperature is 2000 K; therefore, the goal of equilibration is to achieve an equilibrated system at this temperature without any reactions having occurred. The first step of the two-step procedure involves equilibrating the system at 1500 K for 100 ps. This temperature was chosen so that the system could be equilibrated for a reasonable amount of time without thermal decomposition. The second step involves scaling the atomic velocities to achieve a system temperature of 2000 K and then further equilibrating the system for 10 ps. This time was limited by thermal decomposition. Scaling the velocities keeps the partitioning of kinetic energies between translational, rotational, and vibrational motion unchanged. An analysis of this method is presented for the pentamethylheptane–oxygen system used to investigate combustion (see Sec. II C for additional details).

Figure 5 compares the two-step process with method B, which involves equilibrating the system at the target temperature of 2000 K for 10 ps. Figure 5(b) shows that the potential energy is continually increasing with method B, highlighting how 10 ps is insufficient to equilibrate the system from the minimized state. The potential energy is better equilibrated with the two-step process after 10 ps at 2000 K because the system has had time to relax to equilibrium at 1500 K first. Due to the action of the NH thermostat, the system temperature aligns with the target temperature of 2000 K, on average, with both the two-step equilibration procedure and method B [see Fig. 5(a)]. It is, however, essential to check whether the kinetic energy in the system is correctly equipartitioned over the translational, rotational, and vibrational degrees of freedom since each of these kinetic energies has their own effects on reaction kinetics.[41]

Figure 6 presents the translational, rotational, and vibrational temperatures, computed using Eq. (14), which should equal the target temperature on average for an equilibrated system. At the end of equilibration with method B, the translational and rotational temperatures are too hot relative to 2000 K, while the vibrational temperature is too cold, although all three temperatures are moving toward the target temperature of 2000 K. Looking at step 1 of the two-step process, all three temperatures are well equilibrated at 1500 K after around 40 ps. After the atomic velocities are scaled at the end of step 1 to increase the system temperature to 2000 K, the translational and rotational temperatures quickly become too hot and the vibrational temperature becomes too cold. This reveals

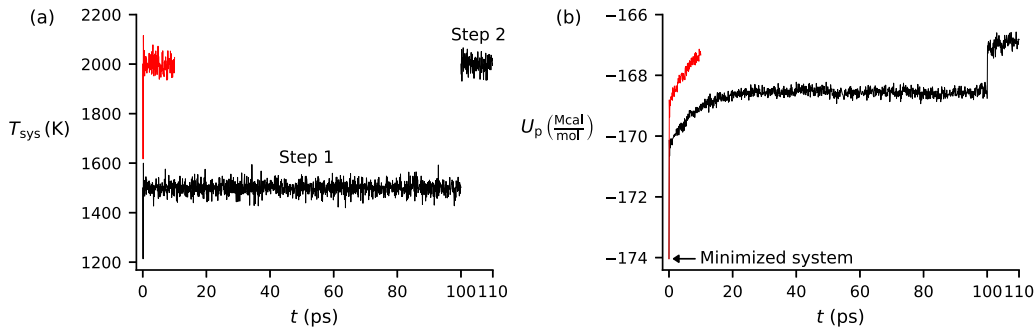


FIG. 5. (a) System temperature and (b) potential energy with a two-step equilibration procedure (black) and method B (red). Charges were computed with QEq, and thermostatting was performed with the NH thermostat.

06 May 2025 09:58:34

© Author(s) 2025

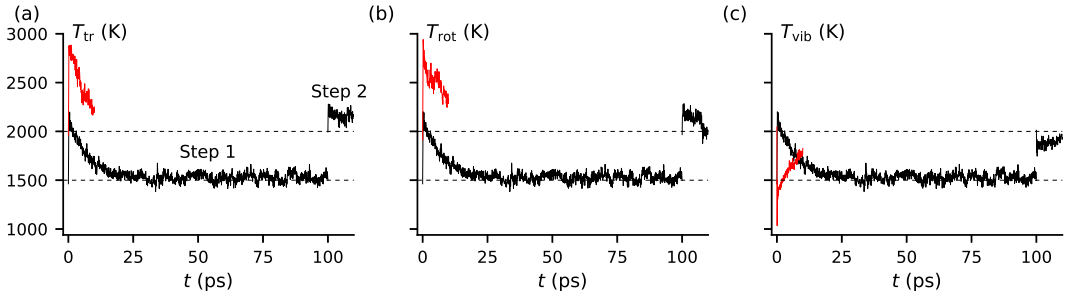


FIG. 6. (a) Translational, (b) rotational, and (c) vibrational temperatures computed over all species with a two-step equilibration procedure (black) and method B (red). Charges were computed with QEq, and thermostatting was performed with the NH thermostat.

the main issue with method A: the potential energy is equilibrated according to a lower temperature than the target temperature, which causes the kinetic energies to become non-equipartitioned after the atomic velocities are scaled upward to reach the target temperature. It is because more of the vibrational kinetic energy is transformed to potential energy compared to the translational and rotational kinetic energies that the vibrational temperature becomes colder than 2000 K after the global action of the NH thermostat, while the translational and rotational temperatures become hotter than 2000 K. Nevertheless, the deviation of these three temperatures from 2000 K is around 200 K at the start of step 2 compared with almost 1000 K at the start of method B. The temperatures are also closer to the target temperature of 2000 K at the end of step 2 compared to at the end of method B. The system is, however, not fully equilibrated by the end of step 2 and should be further equilibrated, with the maximum time set by when the first fuel molecule decomposes. Depending on the molecules in the system under investigation and the target temperature, it is possible that the system could be equilibrated for significantly longer than 10 ps in step 2.

Overall, the two-step process can produce a more equilibrated system than the two methods widely used in the literature. It is possible that adding additional steps at intermediate temperatures between the equilibration temperature of step 1 and the target temperature and also maximizing the time of equilibration at the target temperature before thermal decomposition occurs could allow for complete equilibration at high target temperatures.

V. COMBUSTION WITH REACTIVE MOLECULAR DYNAMICS

Here, the combustion of pentamethylheptane ($C_{12}H_{26}$) in oxygen as predicted by reactive MD is analyzed and discussed.

A. Charge effects: QEq vs QTPIE

Figure 7 presents the time evolution of the number of fuel and oxygen molecules for NVT-MD simulations with the NH thermostat. The time evolution of the number of fuel and oxygen molecules is relatively similar for QEq and QTPIE during the initial 0.5 ns, with minimal oxidation occurring during this time. At t = 0.5 ns, the most abundant species for both QEq and QTPIE are the alkenes C_3H_6 and C_4H_8 and the radicals CH_3 and C_4H_9 (in agreement with the experimental findings of Guzman *et al.*[45] and Liang *et al.*[69]), which form from the decomposition of pentamethylheptane molecules. Figure 7(b) shows that intermediates are more rapidly oxidized with

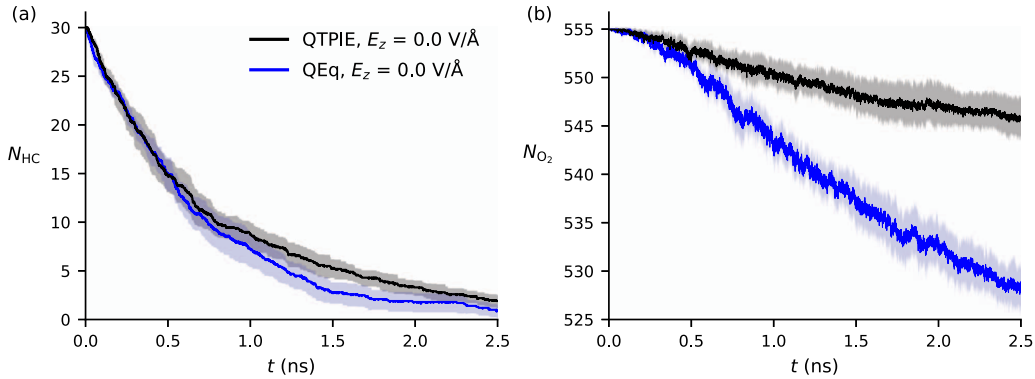


FIG. 7. (a) Number of $C_{12}H_{26}$ and (b) O_2 molecules vs time with charges computed using QEq and QTPIE. The simulations were performed at 2000 K with the NH thermostat. The solid lines are the mean number of molecules over 10 simulations and the shaded regions are 90% confidence intervals for the mean, which were computed using the t-distribution.

06 May 2025 09:58:34

© Author(s) 2025

TABLE II. First-order rate constants for $C_{12}H_{26}$ (k_{HC}) and O_2 (k_{O_2}) for all investigated cases. The time interval from 0 to t_e was used when computing the rate constants. R^2 is the coefficient of determination of the linear fit used to compute the rate constants.

q-method	Thermostat/NVE	E_z (V/Å)	t_e (ns)	k_{HC} (s^{-1})	R^2_{HC}	k_{O_2} (s^{-1})	$R^2_{O_2}$
QEq	NH	0.0	2.00	1.50×10^9	0.996	2.33×10^7	0.991
QTPIE	NH	0.0	1.75	1.11×10^9	0.990	8.48×10^6	0.988
QEq	CSVR	0.0	2.00	1.52×10^9	0.998	2.27×10^7	0.993
QTPIE	CSVR	0.0	2.50	9.89×10^8	0.998	6.23×10^6	0.976
QEq	NVE	0.0	2.00	1.03×10^9	0.996	1.67×10^7	0.992
QTPIE	NVE	0.0	2.00	5.26×10^8	0.994	3.51×10^6	0.943
QEqR	NH	0.05	2.50	9.58×10^8	0.998	1.71×10^7	0.994
QEqR	CSVR	0.05	2.50	1.03×10^9	0.990	1.64×10^7	0.992
QTPIE	NH	0.05	2.50	1.39×10^9	0.996	6.96×10^6	0.981
QTPIE	NH	0.2	2.50	1.25×10^9	0.998	6.19×10^6	0.989
QTPIE	CSVR	0.05	2.00	1.18×10^9	0.997	6.69×10^6	0.981
QTPIE	NVE	0.05	2.00	7.42×10^8	0.993	3.20×10^6	0.907
QEqR	NVE	0.05	0.10	3.74×10^{10}	0.814	2.46×10^8	0.787

QEq compared with QTPIE. This also occurs with CSVR, as shown in Fig. 19 of Appendix E. Faster oxidation occurs with QEq because QEq leads to molecules with sizable net charges, as discussed in Sec. III C, resulting in stronger Coulombic interactions between intermediates and oxygen molecules and, therefore, faster oxidation. From the charge analysis presented in Sec. III C, it is likely that QEq overestimates the strength of Coulombic interactions between intermediates and oxygen molecules and that QTPIE underestimates these interactions. Therefore, it is expected that the true behavior lies between the QEq and QTPIE results presented in Fig. 7.

The first-order rate constants for the consumption of pentamethylheptane (k_{HC}) and oxygen (k_{O_2}) for each case studied are provided in Table II. The consumption of fuel and oxygen is slower with QTPIE when using the CSVR thermostat compared with the NH thermostat (k_{HC} decreases from 1.11×10^9 to 9.89×10^8 s^{-1} and k_{O_2} decreases from 8.48×10^6 s^{-1} to 6.23×10^6 s^{-1}), which suggests that the thermostats directly affect reactions.

The corresponding results with NVE-MD are shown in Fig. 8. The difference between the time evolution of fuel molecules when comparing QEq and QTPIE is larger when no thermostat is used: the ratio of k_{HC} with QEq to k_{HC} with QTPIE increases from 1.35 with the NH thermostat to 2.0 with NVE-MD. With NVE-MD, the temperature of the system initially falls due to decomposition reactions, since they are endothermic, and starts to increase once oxidation begins. The system temperature increases more significantly with QEq compared to QTPIE because more oxidation occurs with QEq, as was the case with NVT-MD. The deviation in the system temperature from 2000 K partly explains the larger differences between the time evolution of species when comparing QEq and QTPIE with NVE-MD compared with NVT-MD. In addition, global thermostats can lead to artificial changes in reactions by artificially redistributing kinetic energy around the system,[41,43] which may contribute to the larger differences between QEq and QTPIE with NVE-MD. For example, consider the thermal decomposition of a

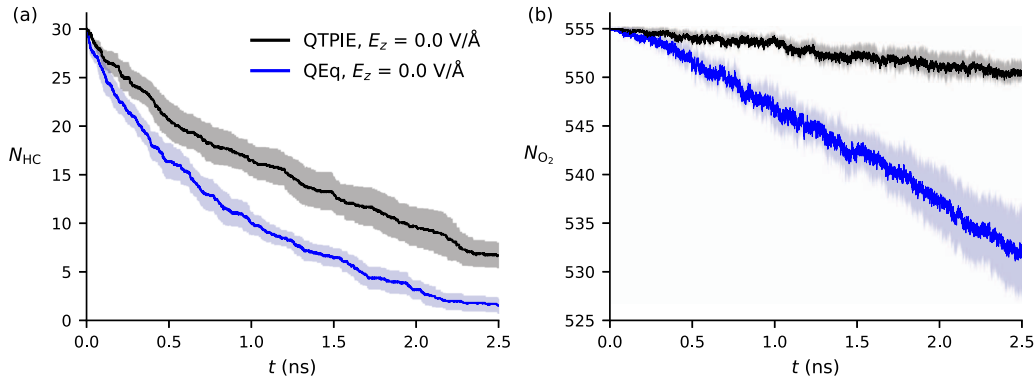


FIG. 8. (a) Number of $C_{12}H_{26}$ and (b) O_2 molecules vs time with charges computed using QEq and QTPIE. The simulations were performed with NVE-MD. The solid lines are the mean number of molecules over 10 simulations and the shaded regions are 90% confidence intervals for the mean, which were computed using the t-distribution.

06 May 2025 09:58:34

© Author(s) 2025

pentamethylheptane molecule by the homolytic cleavage of a C–C bond,[70] which is an endothermic reaction. Following this reaction, a global thermostat such as the NH thermostat or the CSVR thermostat would scale the velocities of all atoms in the system upward, leading to the atoms in the vicinity of the decomposition reaction being colder than the target temperature and the atoms in other parts of the system being hotter than the target temperature.[41] Consequently, when a hydrocarbon molecule thermally decomposes in one part of the molecular system, a global thermostat increases the likelihood of a decomposition event in another part of the system. In this scenario, the global thermostat effectively acts as an artificial catalyst for decomposition reactions. It should be added that the effect of global thermostats on combustion is more complicated than this since both endothermic and exothermic reactions occur throughout combustion. These thermostat artifacts do not occur with NVE-MD, but, of course, the system temperature cannot be controlled without the use of a thermostat.

B. Electric field effects with global thermostats

1. QEq and QEqR

Given that QEq leads to molecules with sizable net charges, as discussed in Sec. III C, it was expected that applying an electric field with QEqR would cause molecules in the system to translate and possibly rotate, leading to an increase in collisions and, therefore, faster reactions. Figure 9 shows that NVT-MD with the NH thermostat actually predicts the opposite effect: an external electric field causes k_{HC} to fall from 1.5×10^9 to 9.58×10^8 s^{-1} and k_{O_2} to fall from 2.33×10^7 to 1.71×10^7 s^{-1}. An external electric field also slows down reaction rates with CSVR (see Fig. 20 of Appendix E).

Studying the partitions of the system's kinetic energy provides some insights into why these NVT-MD simulations predict that an external electric field slows down pentamethylheptane breakdown and oxidation. Figures 10(a)–10(c) show that the translational, rotational, and vibrational temperatures computed over all species are well equipartitioned when no external electric field is applied: the time averages are all ~2000 K. The slight deviation of 3.6 K for rotational motion and 2.8 K for vibrational motion may be because the system was not fully equilibrated at the start, as discussed in Sec. IV. With an external electric field, the translational and rotational temperatures averaged over time increase by 162.0 and 58.2 K, respectively, while the vibrational temperature falls by 112.7 K. The sizable reduction in vibrational temperature occurs because global thermostats enforce

$$K_{tr} + K_{rot} + K_{vib} = K_{sys} \quad \text{where} \quad K_{sys} = \frac{1}{2}(3N - 3)k_B T_{sys}. \tag{15}$$

As a result, an increase in any one of the translational, rotational, or vibrational kinetic energies must come at the expense of at least one of the other kinetic energies. Global thermostats effectively remove the energy introduced by the electric field too quickly such that there can only be a redistribution of kinetic energies and not an increase in the kinetic energies of some degrees of freedom independent of the kinetic energies of other degrees of freedom.

In these simulations, the electric field forces the molecules in the system to translate because of the spurious net charges predicted by QEq. This causes the translational kinetic energy of the molecules in the system to increase, as shown in Fig. 10(d) for pentamethylheptane molecules and in Fig. 10(g) for oxygen molecules. There is also an increase in the rotational kinetic energy of the pentamethylheptane and oxygen molecules [see Figs. 10(e) and 10(h)]. According to Eq. (15), the vibrational kinetic energy must fall to counteract the increase in translational and rotational kinetic energies. This is problematic because each of the translation, rotational, and vibrational kinetic energies affects reaction rates in their own way.[41] For example, an increase in vibrational kinetic energy generally increases reaction rates.[71] The effect seen here when using global thermostats with an external electric field is rather similar to the *flying ice cube effect*, an artifact sometimes caused by velocity rescaling thermostats in which the kinetic energy artificially drains from fast modes of motion (vibration) to slow modes of motion (translation and rotation).[41,56] The vibrational temperature of pentamethylheptane molecules falls by 48.2 K when an electric field is applied, resulting in molecules that are more resistant to thermal decomposition. Furthermore, there is a significant decrease in the vibrational temperature of oxygen molecules: the decrease is around 26% of the temperature when no electric field is applied. This has the effect of stabilizing the oxygen molecules and decelerating

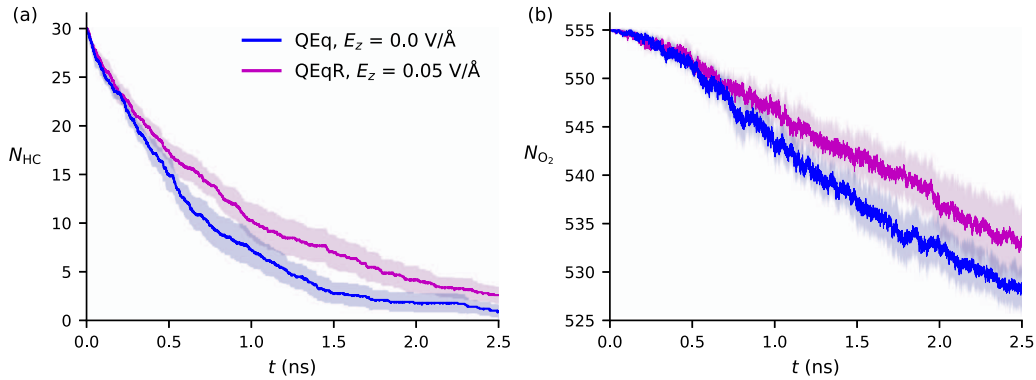


FIG. 9. (a) Number of $C_{12}H_{26}$ and (b) oxygen molecules vs time with QEq and QEqR. These simulations were performed at 2000 K with the NH thermostat. The solid lines are the mean number of molecules over 10 simulations and the shaded regions are 90% confidence intervals for the mean, which were computed using the t-distribution.

06 May 2025 09:58:34

© Author(s) 2025

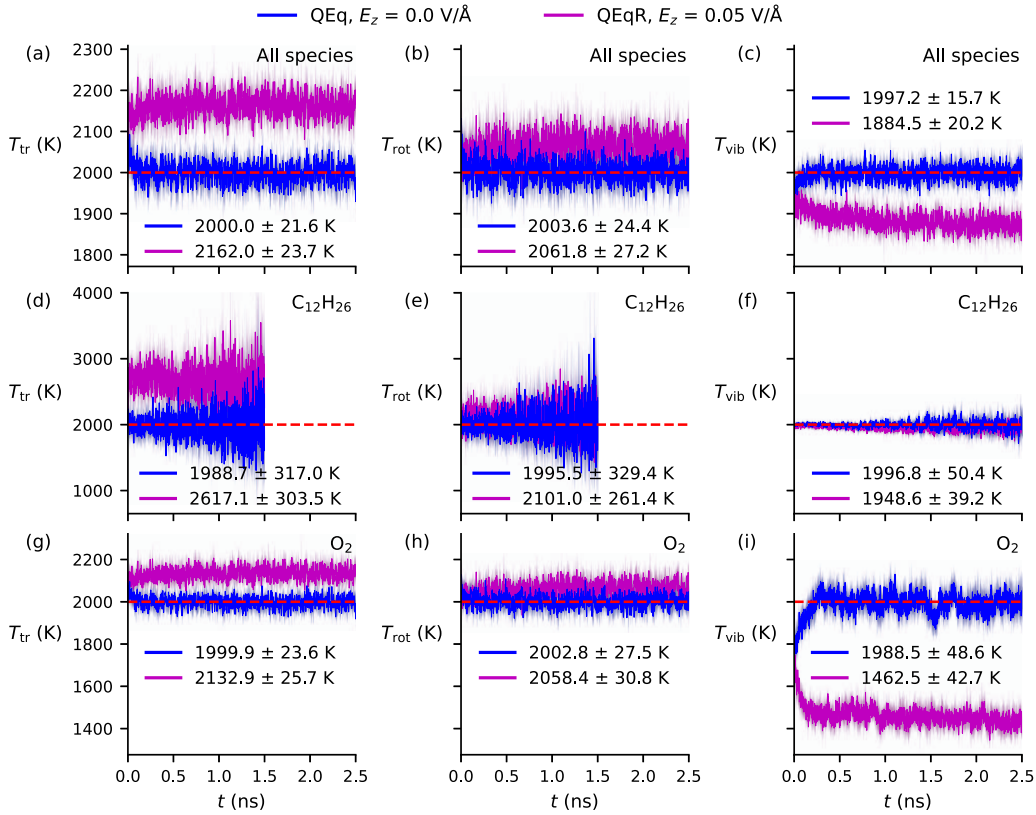


FIG. 10. Translational, rotational, and vibrational temperatures of (a)–(c) all species, (d)–(f) $C_{12}H_{26}$ molecules, and (g)–(i) oxygen molecules vs time with QEq and QEqR. These simulations were performed at 2000 K (marked with a red dashed line) with the NH thermostat. The solid lines are the mean temperatures over 10 simulations and the shaded regions are 90% confidence intervals for the mean, which were calculated using the t-distribution. The numbers shown in each subfigure are the mean temperatures averaged over time ± the standard deviation. The temperatures are not plotted beyond 1.5 ns in (d) and (e) because the limited number of remaining degrees of freedom leads to large temperature fluctuations.

oxidation. It is, therefore, sensible to conclude that the electric field effects shown in Figs. 9 and 20 are artifacts arising from the use of global thermostats with external electric fields. It is unfortunately common practice to use global thermostats with external electric fields,[13–22] and it is likely that these artifacts have affected the results presented and conclusions drawn in a number of previous studies, not just those investigating electric field effects on combustion chemistry. Greater care should be taken when using methods designed for equilibrium simulations, like the NH and CSVR thermostats, in a non-equilibrium setting.

2. QTPIE

With QTPIE, there are only small differences in the time evolution of the fuel and oxygen molecules when an electric field of strength E_z = 0.05 V/Å is applied compared with the zero-field case (see Fig. 11), although there is, perhaps, slightly faster fuel consumption beyond ~1.0 ns with the external electric field. This is, for the most part, expected since QTPIE predicts small molecular net charges and smaller than expected atomic partial charges, as discussed in Sec. III C. To see if any flying-ice-cube-like artifacts arise with even stronger electric fields, we also investigated E_z = 0.2 V/Å. Although it is common practice to employ fields of this strength and stronger,[22] we reiterate that one should generally stick to the upper limit of 0.05 V/Å recommended by English and Waldron.[42] With E_z = 0.2 V/Å, the time evolution of the number of pentamethylheptane molecules remains largely unchanged. However, there is a slight decrease in the consumption rate of oxygen, with k_{O_2} decreasing from 8.48×10^6 s^{-1} with no electric field to 6.19×10^6 s^{-1} with E_z = 0.2 V/Å.

The kinetic energy analysis shown in Fig. 12 reveals that there is, once again, a redistribution of kinetic energy from vibrational motion to translational and rotational motion when an electric field of strength E_z = 0.2 V/Å is applied. For example, the vibrational temperature of the oxygen molecules averaged over time is 50.0 K smaller when an electric field of strength E_z = 0.2 V/Å is applied, which is the likely explanation of why oxygen molecules are less readily consumed with E_z = 0.2 V/Å. Therefore, even though QTPIE can reduce long-range charge transfer, artifacts still arise with global thermostats, but at stronger electric fields compared with QEqR.

06 May 2025 09:58:34

© Author(s) 2025

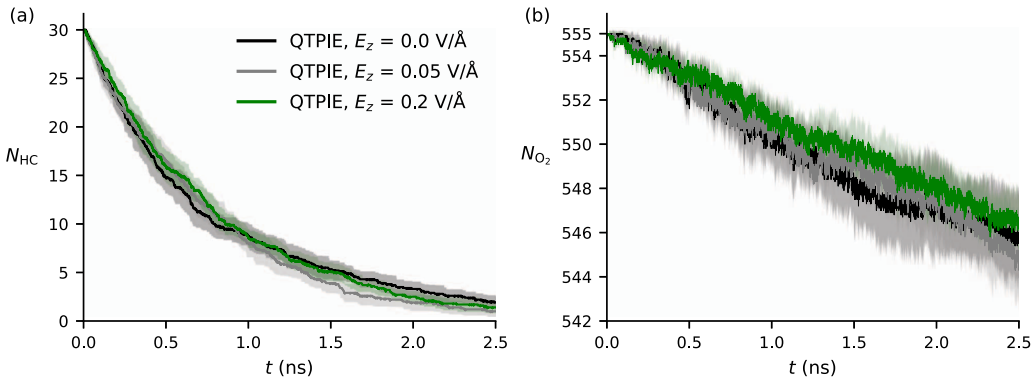


FIG. 11. (a) Number of $C_{12}H_{26}$ and (b) O_2 molecules vs time with QTPIE. The simulations were performed at 2000 K with the NH thermostat. The solid lines are the mean number of molecules over 10 simulations and the shaded regions are 90% confidence intervals for the mean, which were computed using the t-distribution.

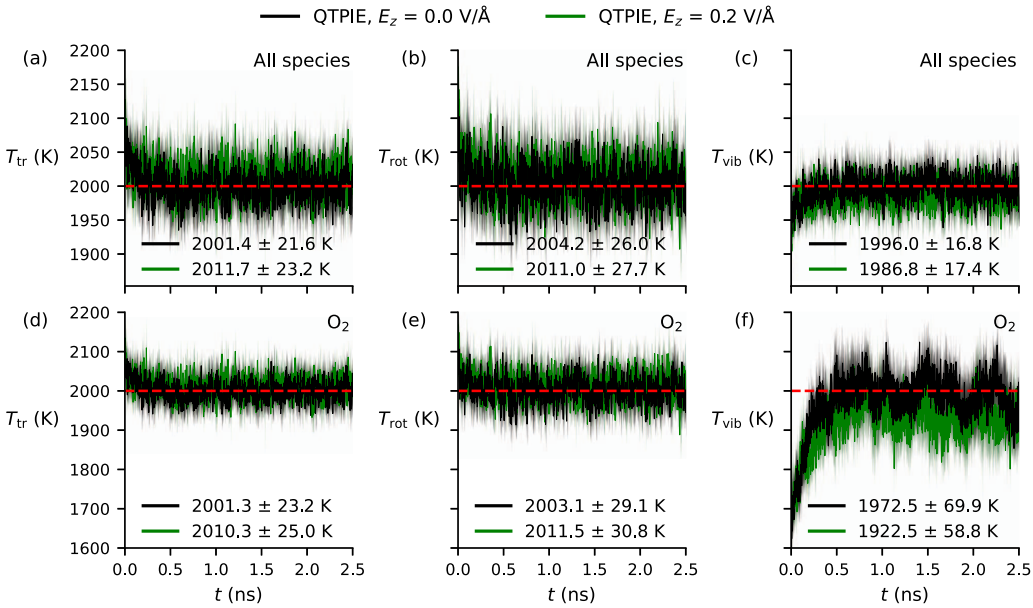


FIG. 12. Translational, rotational, and vibrational temperatures of (a)–(c) all species and (d)–(f) oxygen molecules vs time with QTPIE. The simulations were performed at 2000 K (marked with a red dashed line) with the NH thermostat. The solid lines are the mean temperatures over 10 simulations and the shaded regions are 90% confidence intervals for the mean, which were calculated using the t-distribution. The numbers shown in each subfigure are the mean temperatures averaged over time ± the standard deviation.

C. Electric field effects without thermostatting

NVE-MD simulations were also performed to understand how the effects of an electric field change when no thermostat is used.

1. QTPIE

Figure 13 shows that there is a significant increase in the rate of consumption of pentamethylheptane when an electric field of strength E_z = 0.05 V/Å is applied when using NVE-MD, which differs from the NVT-MD predictions. In particular, k_{HC} increases from 5.26×10^8 s^{-1} with no external electric field to 7.42×10^8 s^{-1} with E_z = 0.05 V/Å. There does not appear to be a significant change in the consumption of oxygen, although the consumption of oxygen may be significantly faster with an external electric field over times much longer than 2.5 ns.

A kinetic energy analysis was performed to better understand the effects of the electric field on the system. Figure 14 clearly shows that energy introduced into the system by the electric field increases the system temperature and the translational, rotational, and vibrational temperatures computed over all species. There are similar temperature increases when considering the kinetic energies of the fuel and oxygen separately. As time progresses, the electric field continues to impart energy to the system and the difference in temperature relative to the zero-field case continually increases. This

06 May 2025 09:58:34

© Author(s) 2025

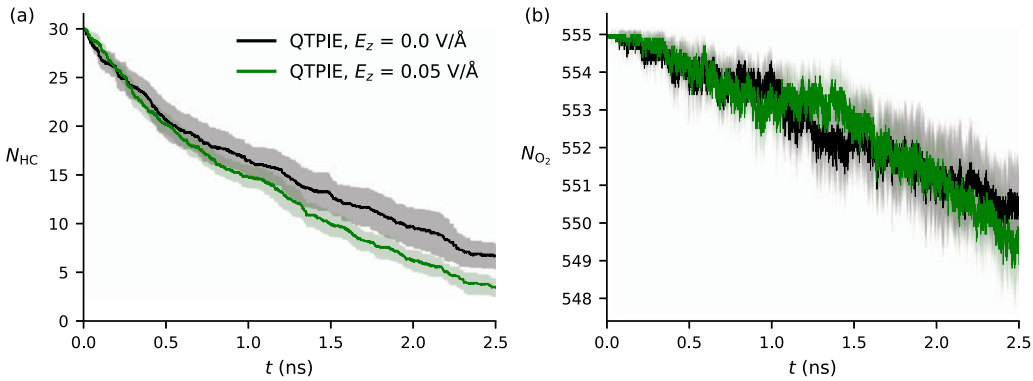


FIG. 13. (a) Number of $C_{12}H_{26}$ and (b) O_2 molecules vs time with QTPIE. The simulations were performed with NVE-MD. The solid lines are the mean number of molecules over 10 simulations and the shaded regions are 90% confidence intervals for the mean, which were computed using the t-distribution.

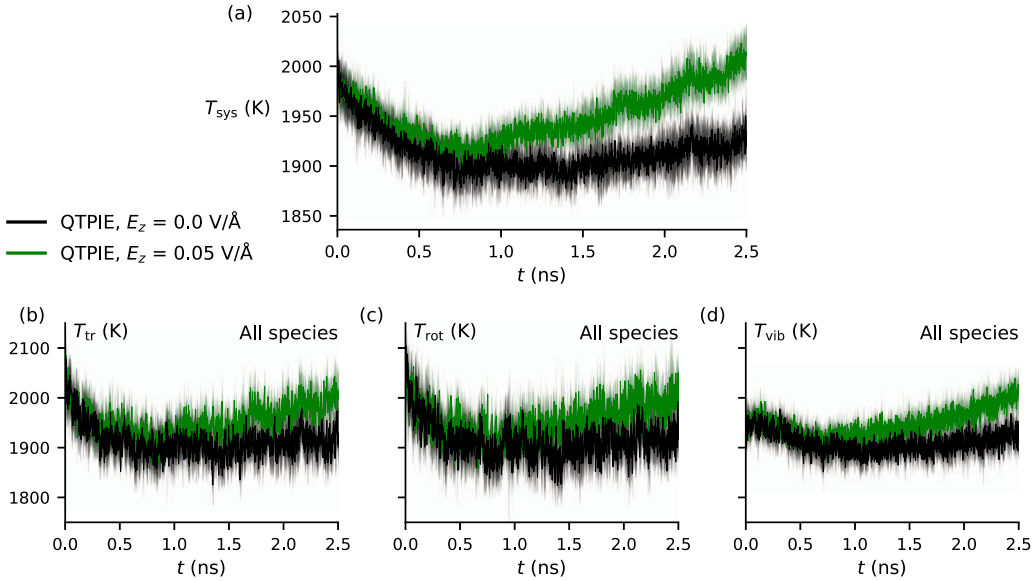


FIG. 14. (a) System temperature and (b)–(d) the translational, rotational, and vibrational temperatures, respectively, of all species vs time with QTPIE. The simulations were performed with NVE-MD. The solid lines are the mean temperatures over 10 simulations and the shaded regions are 90% confidence intervals for the mean, which were calculated using the t-distribution.

highlights the key issue with not using a thermostat at all when imposing an external electric field: the energy introduced into the system by the electric field cannot be dissipated as heat, which leads to continual heating.[42] In other words, the system is adiabatic with NVE-MD. Despite this, the effects of an external electric field on chemical reactions are more realistic with NVE-MD compared with NVT-MD, provided that the amount of field-induced heating is not excessive, as NVE-MD avoids flying-ice-cube-like artifacts and other artificial effects from global thermostats on chemical reactions. Furthermore, the rate of field-induced heating would be smaller with a method that can eliminate long-range charge transfer entirely and provide neutral molecules.

2. QEq and QEqR

Field-induced heating is expected to occur significantly faster with QEqR compared with QTPIE because QEq leads to molecules with large net charges. Figure 15(a) shows that there is a rapid increase in the system temperature from 2000 to 4500 K in just 0.15 ns when an electric field is applied with QEqR. Furthermore, Figs. 15(b) and 15(c) show that there is a rapid decomposition of the pentamethylheptane molecules and a rapid consumption of the oxygen molecules compared to the zero-field case. The first of the 10 simulations failed after 147 ps, and all 10 simulations failed by 179 ps. Presumably, the time step used in the simulations should be

06 May 2025 09:58:34

© Author(s) 2025

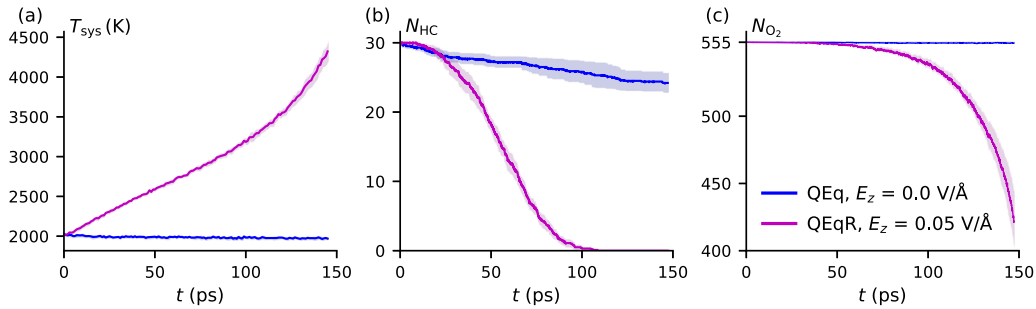


FIG. 15. (a) System temperature, (b) the number of $C_{12}H_{26}$ molecules, and (c) the number of O_2 molecules vs time with QEq and QEqR. The simulations were performed with NVE-MD. The solid lines are the mean values over 10 simulations and the shaded regions are 90% confidence intervals, which were computed using the t-distribution.

reduced to below 0.1 fs once the system temperatures exceed 4000 K. It is evident that NVT-MD and NVE-MD lead to largely different electric field effects on the combustion of pentamethylheptane with QEqR; however, neither NVT-MD nor NVE-MD provides a realistic description of electric field effects with QEqR because of the unphysical net molecular charges predicted by QEq and, therefore, by QEqR.

D. Alternative methods for temperature control

It may be desirable to control the system temperature to better replicate experimental conditions, for example, without introducing artificial changes to chemical reactions that arise when using a global thermostat.

Removing the translational and rotational motion of molecules before thermostatting so that the global thermostat in use only operates on the vibrational motion of atoms[55] could prevent the flying-ice-cube-like artifacts that arose when applying an external electric field with a global thermostat. A practical implementation of this method is complicated, however, since bonds are not fixed in reactive MD, which makes it difficult to avoid introducing additional artifacts due to the incorrect identification of bonds.

It may be worth investigating different values for the damping parameter used by the NH and CSVR thermostats. A value of 200 fs was used in this study, as is typical.[19] Increasing the value of the damping parameter used is expected to reduce artificial effects from the thermostat but at the expense of temperature control.[43]

A promising alternative approach could be to control the temperature of the reactive system indirectly through an inert carrier gas.[41,43] With this approach, the inert carried gas is advanced using NVT-MD and the reactive system is advanced using NVE-MD. The aim of this approach is to allow the reactive system to evolve naturally, without a thermostat artificially affecting reactions, and to approximately control the temperature of the reactive system by allowing energy to transfer between the inert and reacting systems. This approach does come with an increased computational cost and requires the strength of non-bonded interactions between the atoms of the reactive system and the inert system to be specified. Investigating this approach further will be the focus of future work.

VI. CONCLUSIONS

Most studies use QEq when studying fuel combustion with reactive MD through ReaxFF even though it is well known that QEq leads to spurious long-range charge transfer. In addition, most studies appear to start combustion simulations from a non-equilibrated system and fail to comment on how the initial deviation from equilibrium influences reaction rates. It is also common practice to use a global thermostat when simulating the effects of an external electric field on combustion, without first analyzing how the thermostat affects chemical reactions. This study analyzes these critical aspects of the reactive MD methodology in the context of hydrocarbon combustion in an external electric field.

For the fuel–oxygen system investigated, QEq leads to inaccurate charges with the fuel and oxygen molecules acquiring net charges of $1.11e$ and $-0.06e$, on average, respectively. QTPIE is effective at reducing long-range charge transfer and predicting almost neutral molecules but achieves this at the penalty of underestimating the magnitude of some atomic partial charges. QEq leads to faster fuel consumption and oxidation of intermediates compared with QTPIE because of the larger atomic partial charges predicted by QEq. Although QTPIE may provide sufficient accuracy for the molecular system of interest, future work should be conducted to parameterize ReaxFF with a more accurate method for computing atomic partial charges, such as ACKS2, to allow reactions to be more accurately simulated.

The electric field implementation in QEqR and QTPIE, which involves electric potential differences, is based on intuition, rather than being rigorously derived, and is beneficial because it permits periodic boundaries in the direction of an external electric field. There is also the opportunity to tune the scaling factor β during ReaxFF training so that QEqR and QTPIE can more accurately describe electric polarization. QEqR is also advantageous over QEqA in that it does not worsen long-range charge transfer. With both QEqA and QEqR, however, the effect of the electric field on the molecules in the system is heavily influenced by the spurious net molecular charges predicted by QEq. This is less of an issue with QTPIE, although molecular drift in the electric field due to the net charges of molecules is still expected with QTPIE but at longer simulation times or with stronger external electric fields compared with QEqA and QEqR.

06 May 2025 09:58:34

© Author(s) 2025

The presented equilibration analysis highlights that the two methods widely used by previous studies do not provide well-equilibrated systems at the target temperature. In particular, the kinetic energies are not equipartitioned over the translational, rotational, and vibrational motions, which directly affects reaction kinetics. Employing a two-step equilibration procedure can provide a more, although not fully, equilibrated system under the constraint on the equilibration time imposed by thermal decomposition. Extending this procedure to more than two steps could lead to even better system equilibration.

When an electric field acts to increase the translational and rotational kinetic energies of molecules, global thermostats sacrifice vibrational kinetic energy to maintain the system temperature. This leads to an artificial freezing of bonds, in a similar manner to the flying ice cube effect, and inevitably affects reaction kinetics. For example, an electric field of strength $E_z = 0.05$ V/Å results in a significant decrease in fuel consumption and oxidation with QEqR with both the NH and CSVR thermostats. This simulation artifact also affects reaction kinetics with QTPIE, as QTPIE cannot prevent long-range charge transfer entirely, but at stronger electric fields compared with QEqR. Given the widespread use of global thermostats with external electric fields in (reactive) MD, it is likely that similar artifacts have affected the results and conclusions of previous studies. NVE-MD avoids artificial effects from thermostats but cannot dissipate the energy introduced into the system by the electric field, which can lead to substantial heating. With a method that can predict neutral species, such as ACKS2, heating will occur more slowly and NVE-MD should be preferred over NVT-MD. Alternative approaches to global thermostatting should be pursued that can provide temperature control with an external electric field without introducing artificial behavior.

ACKNOWLEDGMENTS

The authors thank Efstratios Kritikos for useful information regarding the implementation of QTPIE in LAMMPS and the Imperial College Research Computing Service (https://doi.org/10.14469/hpc/2232) for computational resources.

This work was performed within the framework of the FFLECS Project funded by the European Union's Horizon Europe research and innovation program under Grant Agreement No. 101096436. Views and opinions expressed are, however, those of the authors only and do not necessarily reflect those of the European Union. Neither the European Union nor the granting authority can be held responsible for them. UK participants in Horizon Europe Project FFLECS are supported by UKRI Grant Nos. 10101902 (Imperial College London) and 10085576 (University of Cambridge).

AUTHOR DECLARATIONS

Conflict of Interest

The authors have no conflicts to disclose.

Author Contributions

Navraj S. Lalli: Conceptualization (equal); Formal analysis (lead); Investigation (lead); Methodology (lead); Software (lead); Writing – original draft (lead); Writing – review & editing (equal). **Andrea Giusti**: Conceptualization (equal); Funding acquisition (lead); Methodology (supporting); Supervision (lead); Writing – review & editing (equal).

DATA AVAILABILITY

The data that support the findings of this study are openly available in Zenodo at https://doi.org/10.5281/zenodo.15222653.

APPENDIX A: IMPLEMENTATION OF `fix qtpie/reaxff`

`fix qtpie/reaxff` uses the overlap integral between two normalized spherically symmetric 1s Gaussian-type orbitals for S_{ij} in Eq. (5),[72]

$$S_{ij} = \left(\frac{4\alpha_i\alpha_j}{(\alpha_i+\alpha_j)^2}\right)^{\frac{3}{4}} \exp\left(-\frac{\alpha_i\alpha_j}{\alpha_i+\alpha_j} r_{ij}^2\right), \tag{A1}$$

where α_i is the Gaussian orbital exponent of the ith atom. With Eq. (A1), $S_{ij} = 0$ for two infinitely separated atoms and $S_{ii} = 1$. The orbital exponents provide an additional parameter that can be optimized during the parameterization of ReaxFF, which could improve the accuracy of charge computations. The same Gaussian orbital exponent is used for all atoms of the same type (e.g., the same Gaussian orbital exponent is used for all hydrogen atoms, regardless of chemical environment). The use of orbital exponents is also advantageous in that a cutoff radius, r_{ocut}, can be defined based on the minimum Gaussian orbital exponent, allowing overlap integrals to be neglected when $r_{ij} \geq r_{\text{ocut}}$. Neglecting overlap integrals when $S_{ij} \leq 10^{-c}$ leads to

$$r_{\text{ocut}} = \sqrt{\frac{2c}{\alpha_{\min}} \ln 10}, \tag{A2}$$

where $\alpha_{\min} = \min\{\alpha_1, \ldots, \alpha_N\}$ and ln is the natural logarithm. This is implemented in `fix qtpie/reaxff` with $c = 10$ to reduce the number of overlap integrals that must be computed. Ghost atoms (atoms owned by other processors and atoms across periodic boundaries that are within a cutoff distance of each processor[35]) are used when computing the overlap integrals and the differences in absolute electronegativities in Eq. (5) to ensure that all nearby atoms are accounted for.

When applying an external electric field, `fix qtpie/reaxff` requires that the electric field is applied to all atoms in the system. This restriction was added to avoid issues when computing $\phi_i - \phi_j$ in Eq. (10), where, for example, atom i is subject to an external electric field and atom j is not. It is unclear how $\phi_i - \phi_j$ should be computed in this case. One option could be to set $\phi_j = 0$, but this would then cause $\tilde{\chi}_{ri}$ to depend on the absolute position of atom i, leading to the same shortcomings that arise with QEqA.

APPENDIX B: KINETIC ENERGY COMPUTATIONS

This section details how the translational, rotational, and vibrational kinetic energies were computed for each molecule in the system by considering one molecule composed of N_{m} atoms. The velocity of the ith atom in the molecule can be expressed as a sum of

06 May 2025 09:58:34

© Author(s) 2025

contributions due to the translation of the molecule's center of mass, rotation of the molecule around its center of mass, and vibration,

$$\boldsymbol{v}_i = \boldsymbol{v}_c + \boldsymbol{\omega} \times \boldsymbol{r}_{ci} + \boldsymbol{u}_i, \tag{B1}$$

where $\boldsymbol{v}_c$ is the velocity of the molecule's center-of-mass, $\boldsymbol{\omega}$ is the angular velocity of the molecule about its center of mass, $\boldsymbol{r}_{ci}$ is the position of the ith atom relative to the center of mass of the molecule, and $\boldsymbol{u}_i$ is the vibrational velocity of the ith atom. Finding each of the velocity components in Eq. (B1) allows the translational, rotational, and vibrational kinetic energies of the molecule to be computed.

We denote the mass of the molecule by

$$m_m = \sum_{i=1}^{N_m} m_i, \tag{B2}$$

where m_i is the mass of the ith atom. The center-of-mass velocity can be found from

$$\boldsymbol{v}_c = \frac{\sum_{i=1}^{N_m} m_i \boldsymbol{v}_i}{m_m}, \tag{B3}$$

and the translational kinetic energy of the molecule follows from

$$K_{tr} = \frac{1}{2} m_m \boldsymbol{v}_c \cdot \boldsymbol{v}_c, \tag{B4}$$

where $\cdot$ denotes the inner product.

In order to compute the angular velocity of the molecule, the center of mass of the molecule, $\boldsymbol{r}_{com}$, must first be computed,

$$\boldsymbol{r}_{com} = \frac{\sum_{i=1}^{N_m} m_i \boldsymbol{r}_{ui}}{m_m}, \tag{B5}$$

where $\boldsymbol{r}_{ui}$ is the position of the ith atom in unwrapped atomic coordinates—unwrapped coordinates must be used so that the center of mass computation is not affected by the wrapping of parts of the molecule over periodic boundaries. The angular momentum of the molecule, $\boldsymbol{L}$, is given by

$$\boldsymbol{L} = \boldsymbol{I}\boldsymbol{\omega}, \tag{B6}$$

where $\boldsymbol{I}$ is the moment of inertia tensor of the molecule. The angular momentum can be computed through

$$\boldsymbol{L} = \sum_{i=1}^{N_m} m_i (\boldsymbol{r}_{ci} \times \boldsymbol{v}_i), \tag{B7}$$

and the moment of inertia tensor in a rectangular Cartesian coordinate system can be computed through

$$\boldsymbol{I} = \begin{pmatrix} \sum_{i=1}^{N_m} (y_{ci}^2 + z_{ci}^2) m_i & -\sum_{i=1}^{N_m} (x_{ci} y_{ci}) m_i & -\sum_{i=1}^{N_m} (x_{ci} z_{ci}) m_i \\ -\sum_{i=1}^{N_m} (y_{ci} x_{ci}) m_i & \sum_{i=1}^{N_m} (x_{ci}^2 + z_{ci}^2) m_i & -\sum_{i=1}^{N_m} (y_{ci} z_{ci}) m_i \\ -\sum_{i=1}^{N_m} (z_{ci} x_{ci}) m_i & -\sum_{i=1}^{N_m} (z_{ci} y_{ci}) m_i & \sum_{i=1}^{N_m} (x_{ci}^2 + y_{ci}^2) m_i \end{pmatrix}, \tag{B8}$$

where $\boldsymbol{r}_{ci} = x_{ci}\boldsymbol{e}_x + y_{ci}\boldsymbol{e}_y + z_{ci}\boldsymbol{e}_z$. When a molecule has a non-singular moment of inertia tensor, the angular velocity of the molecule can be found from Eq. (B6) using the inverse of the moment of inertia tensor,

$$\boldsymbol{\omega} = \boldsymbol{I}^{-1}\boldsymbol{L}. \tag{B9}$$

The rotational kinetic energy of the molecule then follows from

$$K_{rot} = \frac{1}{2}\boldsymbol{L} \cdot \boldsymbol{\omega}. \tag{B10}$$

For molecules with a linear geometry, such as oxygen molecules, the moment of inertia tensor is singular because the moment of inertia about the axis passing through all atoms of the linear molecule is 0; in other words, there is no resistance to rotation about this axis. Equation (B9) can, therefore, not be used with linear molecules. We, instead, computed the angular velocity of a linear molecule by first computing the principal axes ($\{\boldsymbol{e}_1, \boldsymbol{e}_2, \boldsymbol{e}_3\}$) and principal moments of inertia ($\{I_1, I_2, I_3\}$) of the molecule. The axis that passes through all atoms of the linear molecule was used as the first principal axis such that $I_1 = 0$. The Gram–Schmidt process was then used to find two unit vectors that are orthogonal to each other and to the first principal axis, which serve as the other two principal axes. Following this, the principal moments of inertia could be computed since they are the eigenvalues of the eigenvectors given by the principal axes. The angular momentum of a linear molecule can be expressed as

$$\boldsymbol{L} = I_2\omega_2\boldsymbol{e}_2 + I_3\omega_3\boldsymbol{e}_3, \tag{B11}$$

where $\{\omega_1, \omega_2, \omega_3\}$ are the principal angular velocities of the molecule, i.e., $\boldsymbol{\omega} = \omega_1\boldsymbol{e}_1 + \omega_2\boldsymbol{e}_2 + \omega_3\boldsymbol{e}_3$ ($\omega_1 = 0$ for the linear molecule). Following from Eq. (B11),

$$\omega_2 = \frac{\boldsymbol{L} \cdot \boldsymbol{e}_2}{I_2} \quad \text{and} \quad \omega_3 = \frac{\boldsymbol{L} \cdot \boldsymbol{e}_3}{I_3}. \tag{B12}$$

The rotational kinetic energy of the linear molecule can then be found from

$$K_{rot} = \frac{1}{2}\left(I_2\omega_2^2 + I_3\omega_3^2\right), \tag{B13}$$

or by using Eq. (B10), as for a non-linear molecule.

With $\boldsymbol{v}_c$ and $\boldsymbol{\omega}$ known, the vibrational velocity of each atom in the molecule can be computed using Eq. (B1). The vibrational kinetic energy of the molecule then follows from

$$K_{vib} = \frac{1}{2}\sum_{i=1}^{N_m} m_i \boldsymbol{u}_i \cdot \boldsymbol{u}_i. \tag{B14}$$

It was confirmed that

$$K_{tr} + K_{rot} + K_{vib} = \frac{1}{2}\sum_{i=1}^{N_m} m_i \boldsymbol{v}_i \cdot \boldsymbol{v}_i \tag{B15}$$

for each molecule.

The Python code written to perform the kinetic energy analysis is also provided in https://doi.org/10.5281/zenodo.15222653.

06 May 2025 09:58:34

© Author(s) 2025

APPENDIX C: TWO WATER MOLECULES IN AN ELECTRIC FIELD

This section repeats the analysis presented in Ref. 36 of two water molecules in an electric field. The two water molecules were positioned with their oxygen atoms 5 nm apart in the x-direction and 2 Å apart in the z-direction in a cubic domain of side length 10 nm. The second generation ReaxFF water force field was used.[73] After the system was minimized with the oxygen atoms frozen in position, an NVE-MD simulation was performed for 15 ps with no electric field applied and then for 15 ps with an electric field of strength E_z = 0.05 V/Å applied. Periodic boundaries were used in the x- and y-directions, while reflecting boundaries were used in the z-direction to avoid issues with QEqA.

Figure 16 presents the net charge and z-position of the center of mass of each water molecule over time. It is evident from Fig. 16(a) that each water molecule is neutral before an electric field is applied with both QEqA and QTPIE. However, once an electric field is applied, the water molecule with higher initial z-position acquires a net positive charge with QEqA, while the other water molecule acquires an equivalent net negative charge. The same charges are predicted for infinite separation between the water molecules in the x-direction. This behavior is the result of unphysical long-range charge transfer and arises here since χ_a depends on

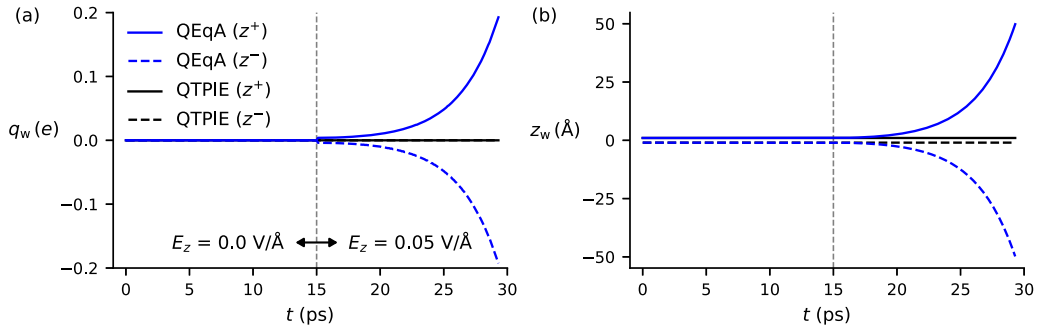


FIG. 16. (a) Net charge and (b) the z-position of the center of mass of two water molecules before and after an electric field is applied with QEqA and QTPIE. In the legend, z^+ and z^- refer to the water molecule with the higher and lower initial z-positions, respectively.

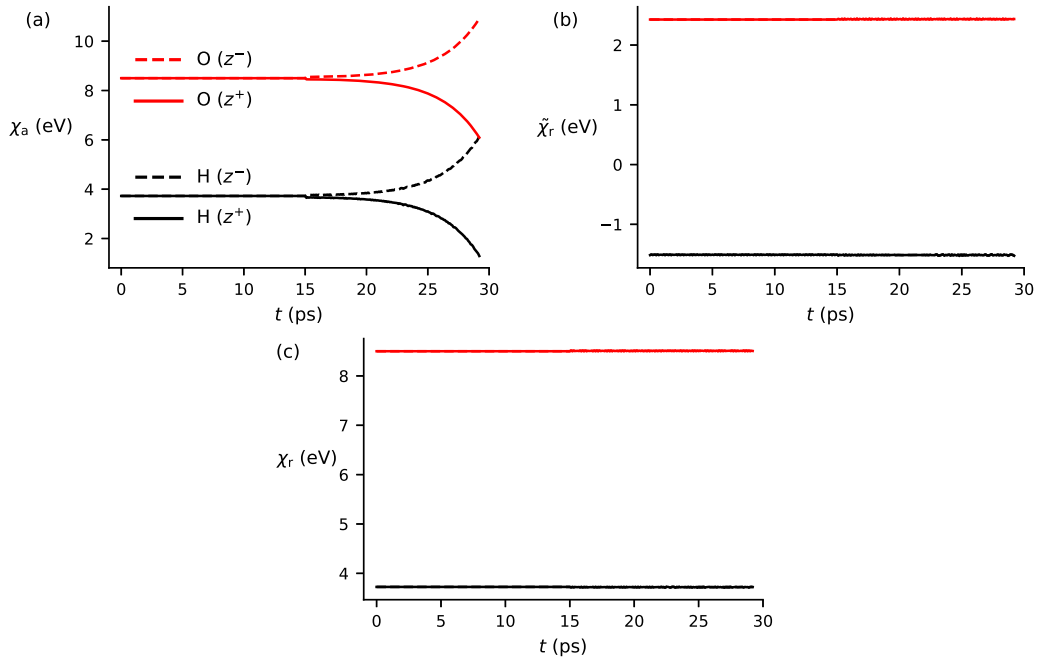


FIG. 17. Effective electronegativities of one oxygen and one hydrogen on each water molecule with (a) QEqA, (b) QTPIE, and (c) QEqR. z^+ and z^- refer to the water molecule with the higher and lower initial z-positions, respectively.

06 May 2025 09:58:34

© Author(s) 2025

absolute atomic positions. These spurious, non-integer net charges cause the two water molecules to translate in the electric field, as shown in Fig. 16(b). It is particularly concerning that the magnitudes of the net charges of the two water molecules continue to increase as the two water molecules translate in the electric field, which occurs because the effective electronegativities χ_a of the atoms on the two water molecules diverge over time [shown in Fig. 17(a)].

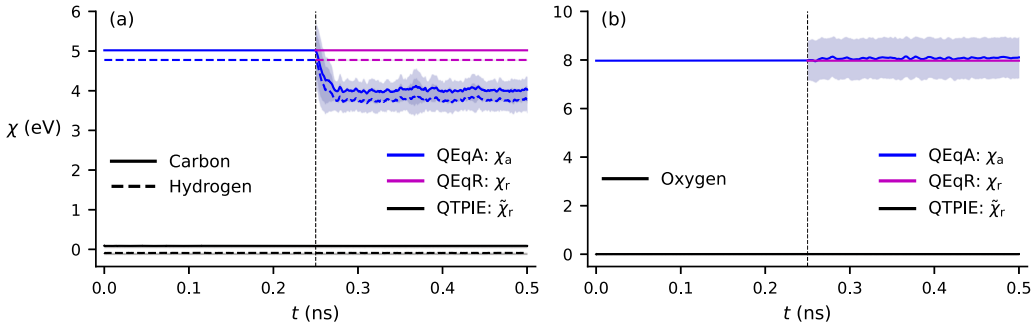


FIG. 18. (a) Effective electronegativities of the carbon and hydrogen atoms in the pentamethylheptane molecules and (b) the oxygen atoms in the oxygen molecules averaged over all atoms of the same type, before and after an electric field is applied at $t = 0.25$ ns, with QEqA, QEqR, and QTPIE. The solid lines show the average over all atoms of each type at each time, and the shaded regions present the standard deviation over all atoms of each type.

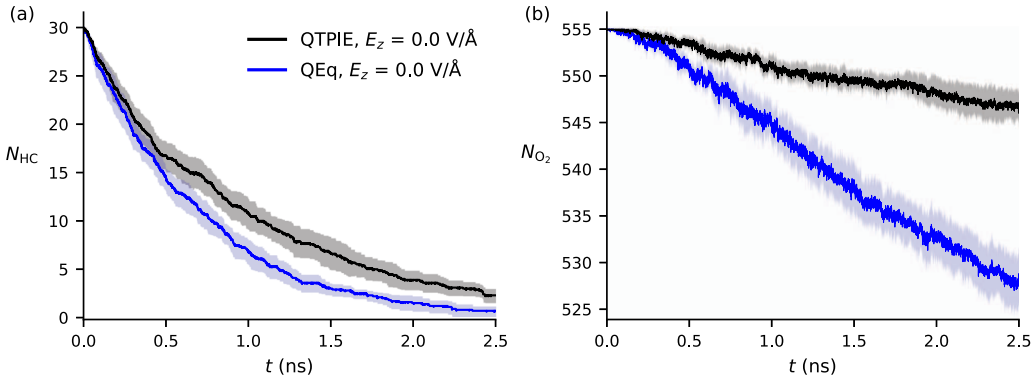


FIG. 19. (a) Number of $C_{12}H_{26}$ and (b) O_2 molecules vs time with atomic charges computed using QEq and QTPIE. The simulations were performed at 2000 K with CSVR. The solid lines are the mean number of molecules over 10 simulations and the shaded regions are 90% confidence intervals for the mean, which were computed using the t-distribution.

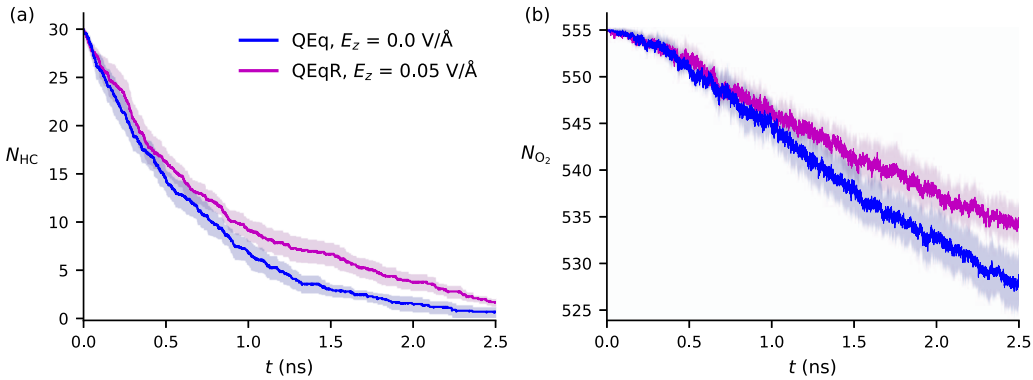


FIG. 20. (a) Number of $C_{12}H_{26}$ and (b) O_2 molecules vs time with QEq and QEqR. These simulations were performed at 2000 K with CSVR. The solid lines are the mean number of molecules over 10 simulations and the shaded regions are 90% confidence intervals for the mean, which were computed using the t-distribution.

06 May 2025 09:58:34

© Author(s) 2025

The expected behavior is that the two water molecules remain neutral[36] and only rotate to orient their dipoles in the direction of the applied electric field, rather than translating. This expected behavior is predicted by QTPIE (the same behavior is also predicted by QEqR), as shown in Fig. 16, and aligns with the predictions of ACKS2 and DFT presented in Ref. 36. QEqR and QTPIE lead to the expected behavior because the effective electronegativities used with these methods, which are shown in Figs. 17(b) and 17(c), are approximately the same for the corresponding atoms on each water molecule with and without an electric field applied.

APPENDIX D: EFFECTIVE ELECTRONEGATIVITIES FOR PENTAMETHYLHEPTANE IN OXYGEN

Figure 18 presents the effective electronegativities of the carbon and hydrogen atoms in the pentamethylheptane molecules and the oxygen atoms in the oxygen molecules.

APPENDIX E: SPECIES ANALYSIS WITH CSVR

Figures 19 and 20 present the number of $C_{12}H_{26}$ and O_2 molecules vs time with atomic charges computed using QEq and QTPIE and with QEq and QEqR, respectively.

REFERENCES

[1] W. F. Lamb, T. Wiedmann, J. Pongratz, R. Andrew, M. Crippa, J. G. J. Olivier, D. Wiedenhofer, G. Mattioli, A. A. Khourdajie, J. House *et al.*, "A review of trends and drivers of greenhouse gas emissions by sector from 1990 to 2018," Environ. Res. Lett. **16**, 073005 (2021).

[2] M. Klöwer, M. R. Allen, D. S. Lee, S. R. Proud, L. Gallagher, and A. Skowron, "Quantifying aviation's contribution to global warming," Environ. Res. Lett. **16**, 104027 (2021).

[3] M. Tamba, J. Krause, M. Weitzel, R. Ioan, L. Duboz, M. Grosso, and T. Vandyck, "Economy-wide impacts of road transport electrification in the EU," Technol. Forecast. Soc. Change **182**, 121803 (2022).

[4] A. R. Gnadt, R. L. Speth, J. S. Sabnis, and S. R. H. Barrett, "Technical and environmental assessment of all-electric 180-passenger commercial aircraft," Prog. Aerosp. Sci. **105**, 1–30 (2019).

[5] A. P. Pires, Y. Han, J. Kramlich, M. Garcia-Perez *et al.*, "Chemical composition and fuel properties of alternative jet fuels," BioResources **13**, 2632 (2018).

[6] D. Vrtiška, P. Vozka, V. Váchová, P. Šimáček, and G. Kilaz, "Prediction of HEFA content in jet fuel using FTIR and chemometric methods," Fuel **236**, 1458–1464 (2019).

[7] M. A. Rendón, C. D. Sánchez R, J. Gallo M, and A. H. Anzai, "Aircraft hybrid-electric propulsion: Development trends, challenges and opportunities," J. Control, Autom. Electr. Syst. **32**, 1244–1268 (2021).

[8] D. Fredrich, E. Weiand, and A. Giusti, "Electrostatic fields for the control of evaporating charged fuel sprays," Int. J. Multiphase Flow **160**, 104312 (2023).

[9] E. Weiand and A. Giusti, "Turbulent dispersion and evaporation of charged nanofuel droplet clouds under the influence of electrostatic fields," Int. J. Spray Combust. Dyn. **16**, 269–289 (2024).

[10] A. Giusti and D. Fredrich, "Fuel effects on the electrostatic control of charged droplet trajectories," Fuel **366**, 131009 (2024).

[11] M. Belhi, B. J. Lee, M. S. Cha, and H. G. Im, "Three-dimensional simulation of ionic wind in a laminar premixed Bunsen flame subjected to a transverse DC electric field," Combust. Flame **202**, 90–106 (2019).

[12] A. C. T. van Duin, S. Dasgupta, F. Lorant, and W. A. Goddard, "ReaxFF: A reactive force field for hydrocarbons," J. Phys. Chem. A **105**, 9396–9409 (2001).

[13] S. Tan, T. Xia, Y. Shi, J. Pfaendtner, S. Zhao, and Y. He, "Enhancing the oxidation of toluene with external electric fields: A reactive molecular dynamics study," Sci. Rep. **7**, 1710 (2017).

[14] C. D. Fu, Y. He, and J. Pfaendtner, "Diagnosing the impact of external electric fields chemical kinetics: Application to toluene oxidation and pyrolysis," J. Phys. Chem. A **123**, 3080–3089 (2019).

[15] X. Jiang, M. Feng, W. Zeng, and K. H. Luo, "Study of mechanisms for electric field effects on ethanol oxidation via reactive force field molecular dynamics," Proc. Combust. Inst. **37**, 5525–5535 (2019).

[16] F. Sun and W. Zeng, "Electric field effects on hydrogen/methane oxidation: A reactive force field based molecular dynamics study," Int. J. Hydrogen Energy **45**, 20194–20199 (2020).

[17] E. Kritikos and A. Giusti, "Reactive molecular dynamics investigation of toluene oxidation under electrostatic fields: Effect of the modeling of local charge distribution," J. Phys. Chem. A **124**, 10705–10716 (2020).

[18] X. Z. Jiang and K. H. Luo, "Reactive and electron force field molecular dynamics simulations of electric field assisted ethanol oxidation reactions," Proc. Combust. Inst. **38**, 6605–6613 (2021).

[19] E. M. Kritikos, A. Lele, A. C. T. van Duin, and A. Giusti, "A reactive molecular dynamics study of the effects of an electric field on n-dodecane combustion," Combust. Flame **244**, 112238 (2022).

[20] Z. Bai, X. Z. Jiang, and K. H. Luo, "Reactive force field molecular dynamics simulation of pyridine combustion assisted by an electric field," Fuel **333**, 126455 (2023).

[21] E. M. Kritikos, A. Lele, A. C. T. van Duin, and A. Giusti, "Atomistic insight into the effects of electrostatic fields on hydrocarbon reaction kinetics," J. Chem. Phys. **158**, 054109 (2023).

[22] M. Yu, R. Lou, H. Li, F. Wang, J. Wang, and K. Wang, "Reactive force field molecular dynamics (ReaxFF-MD) simulation of lignite combustion under an external electric field," Fuel **358**, 130184 (2024).

[23] K. Chenoweth, A. C. T. van Duin, and W. A. Goddard, "ReaxFF reactive force field for molecular dynamics simulations of hydrocarbon oxidation," J. Phys. Chem. A **112**, 1040–1053 (2008).

[24] K. Chenoweth, A. C. T. van Duin, S. Dasgupta, and W. A. Goddard III, "Initiation mechanisms and kinetics of pyrolysis and combustion of JP-10 hydrocarbon jet fuel," J. Phys. Chem. A **113**, 1740–1746 (2009).

[25] S. Agrawalla and A. C. T. van Duin, "Development and application of a ReaxFF reactive force field for hydrogen combustion," J. Phys. Chem. A **115**, 960–972 (2011).

[26] C. Ashraf and A. C. T. van Duin, "Extension of the ReaxFF combustion force field toward syngas combustion and initial oxidation kinetics," J. Phys. Chem. A **121**, 1051–1068 (2017).

[27] C. Ashraf, A. Jain, Y. Xuan, and A. C. T. van Duin, "ReaxFF based molecular dynamics simulations of ignition front propagation in hydrocarbon/oxygen mixtures under high temperature and pressure conditions," Phys. Chem. Chem. Phys. **19**, 5004–5017 (2017).

[28] C. Ashraf, S. Shabnam, A. Jain, Y. Xuan, and A. C. T. van Duin, "Pyrolysis of binary fuel mixtures at supercritical conditions: A ReaxFF molecular dynamics study," Fuel **235**, 194–207 (2019).

[29] H. Kwon, A. Lele, J. Zhu, C. S. McEnally, L. D. Pfefferle, Y. Xuan, and A. C. T. van Duin, "ReaxFF-based molecular dynamics study of bio-derived polycyclic alkanes as potential alternative jet fuels," Fuel **279**, 118548 (2020).

[30] X. Li, M. Zheng, C. Ren, and L. Guo, "ReaxFF molecular dynamics simulations of thermal reactivity of various fuels in pyrolysis and combustion," Energy Fuels **35**, 11707–11739 (2021).

[31] A. Lele, H. Kwon, K. Ganeshan, Y. Xuan, and A. C. T. van Duin, "ReaxFF molecular dynamics study on pyrolysis of bicyclic compounds for aviation fuel," Fuel **297**, 120724 (2021).

[32] R. F. B. Goncalves, B. K. V. Iha, J. A. F. F. Rocco, and A. E. Kuznetsov, "Reactive molecular dynamics of pyrolysis and combustion of alternative jet fuels: A ReaxFF study," Fuel **310**, 122157 (2022).

[33] W. J. Mortier, S. K. Ghosh, and S. Shankar, "Electronegativity-equalization method for the calculation of atomic charges in molecules," J. Am. Chem. Soc. **108**, 4315–4320 (1986).

[34] A. K. Rappe and W. A. Goddard III, "Charge equilibration for molecular dynamics simulations," J. Phys. Chem. **95**, 3358–3363 (1991).

[35] A. P. Thompson, H. M. Aktulga, R. Berger, D. S. Bolintineanu, W. M. Brown, P. S. Crozier, P. J. In't Veld, A. Kohlmeyer, S. G. Moore, T. D. Nguyen *et al.*,

06 May 2025 09:58:34

© Author(s) 2025

"LAMMPS–A flexible simulation tool for particle-based materials modeling at the atomic, meso, and continuum scales," Comput. Phys. Commun. **271**, 108171 (2022).
[36]J. P. Koski, S. G. Moore, R. C. Clay, K. A. O'Hearn, H. M. Aktulga, M. A. Wilson, J. A. Rackers, J. M. D. Lane, and N. A. Modine, "Water in an external electric field: Comparing charge distribution methods using ReaxFF simulations," J. Chem. Theory Comput. **18**, 580–594 (2021).
[37]T. Verstraelen, P. W. Ayers, V. Van Speybroeck, and M. Waroquier, "ACKS2: Atom-condensed Kohn-Sham DFT approximated to second order," J. Chem. Phys. **138**, 074108 (2013).
[38]J. Chen, *Theory and Applications of Fluctuating-Charge Models* (University of Illinois at Urbana-Champaign, 2009).
[39]O. Assowe, O. Politano, V. Vignal, P. Arnoux, B. Diawara, O. Verners, and A. C. T. van Duin, "Reactive molecular dynamics of the initial oxidation stages of Ni(111) in pure water: Effect of an applied electric field," J. Phys. Chem. A **116**, 11796–11805 (2012).
[40]J. Chen and T. J. Martínez, "QTPIE: Charge transfer with polarization current equalization. A fluctuating charge model with correct asymptotics," Chem. Phys. Lett. **438**, 315–320 (2007).
[41]R. Halonen, I. Neefjes, and B. Reischl, "Further cautionary tales on thermostatting in molecular dynamics: Energy equipartitioning and non-equilibrium processes in gas-phase simulations," J. Chem. Phys. **158**, 194301 (2023).
[42]N. J. English and C. J. Waldron, "Perspectives on external electric fields in molecular simulation: Progress, prospects and challenges," Phys. Chem. Chem. Phys. **17**, 12407–12440 (2015).
[43]A. J. Page, T. Isomoto, J. M. Knaup, S. Irle, and K. Morokuma, "Effects of molecular dynamics thermostats on descriptions of chemical nonequilibrium," J. Chem. Theory Comput. **8**, 4019–4028 (2012).
[44]P. Vozka, D. Vrtiška, P. Šimáček, and G. Kilaz, "Impact of alternative fuel blending components on fuel composition and properties in blends with jet A," Energy Fuels **33**, 3275–3289 (2019).
[45]J. Guzman, G. Kukkadapu, K. Brezinsky, and C. Westbrook, "Experimental and modeling study of the pyrolysis and oxidation of an iso-paraffinic alcohol-to-jet fuel," Combust. Flame **201**, 57–64 (2019).
[46]A. Nakano, "Parallel multilevel preconditioned conjugate-gradient approach to variable-charge molecular dynamics," Comput. Phys. Commun. **104**, 59–69 (1997).
[47]R. G. Parr and R. G. Pearson, "Absolute hardness: Companion parameter to absolute electronegativity," J. Am. Chem. Soc. **105**, 7512–7516 (1983).
[48]J. Chen, D. Hundertmark, and T. J. Martínez, "A unified theoretical framework for fluctuating-charge models in atom-space and in bond-space," J. Chem. Phys. **129**, 214113 (2008).
[49]D. J. Griffiths, *Introduction to Electrodynamics* (Pearson, 2013).
[50]J. Chen and T. J. Martínez, "Charge conservation in electronegativity equalization and its implications for the electrostatic properties of fluctuating-charge models," J. Chem. Phys. **131**, 044114 (2009).
[51]T. Gergs, S. Dirkmann, and T. Mussenbrock, "Integration of external electric fields in molecular dynamics simulation models for resistive switching devices," J. Appl. Phys. **123**, 245301 (2018).
[52]S. Nosé, "A molecular dynamics method for simulations in the canonical ensemble," Mol. Phys. **52**, 255–268 (1984).
[53]W. G. Hoover, "Canonical dynamics: Equilibrium phase-space distributions," Phys. Rev. A **31**, 1695 (1985).
[54]G. Bussi, D. Donadio, and M. Parrinello, "Canonical sampling through velocity rescaling," J. Chem. Phys. **126**, 014101 (2007).
[55]J. Wong-Ekkabut and M. Karttunen, "The good, the bad and the user in soft matter simulations," Biochim. Biophys. Acta, Biomembr. **1858**, 2529–2538 (2016).
[56]E. Braun, S. M. Moosavi, and B. Smit, "Anomalous effects of velocity rescaling algorithms: The flying ice cube effect revisited," J. Chem. Theory Comput. **14**, 5262–5272 (2018).
[57]H. M. Aktulga, J. C. Fogarty, S. A. Pandit, and A. Y. Grama, "Parallel reactive molecular dynamics: Numerical methods and algorithmic techniques," Parallel Comput. **38**, 245–259 (2012).
[58]K. A. O'Hearn, V. H. Man, W. Yang, T.-S. Lee, J. Wang, A. C. Van Duin, H. M. Aktulga, and Y. Qi, "A fast and high-quality charge model for the next generation general AMBER force field," J. Chem. Phys. **153**, 114502 (2020).
[59]L. Martínez, R. Andrade, E. G. Birgin, and J. M. Martínez, "PACKMOL: A package for building initial configurations for molecular dynamics simulations," J. Comput. Chem. **30**, 2157–2164 (2009).
[60]R. K. Pathria, *Statistical Mechanics* (Butterworth-Heinemann, 1996), Vol. 45.
[61]P. T. Merz and M. R. Shirts, "Testing for physical validity in molecular simulations," PLoS One **13**, e0202764 (2018).
[62]D. A. McQuarrie, *Statistical Mechanics* (Harper & Row, 1976).
[63]M. Huš and T. Urbic, "Strength of hydrogen bonds of water depends on local environment," J. Chem. Phys. **136**, 144305 (2012).
[64]G. Herzberg, *Electronic Spectra and Electronic Structure of Polyatomic Molecules* (Van Nostrand Reinhold Company, 1966).
[65]M. M. Islam, "Reactive molecular dynamics simulations of lithium secondary batteries-interfaces and electrodes," Ph.D. thesis, The Pennsylvania State University, 2016.
[66]M. M. Ghahremanpour, J. Tirado-Rives, and W. L. Jorgensen, "Refinement of the optimized potentials for liquid simulations force field for thermodynamics and dynamics of liquid alkanes," J. Phys. Chem. B **126**, 5896–5907 (2022).
[67]S. W. I. Siu, K. Pluhackova, and R. A. Böckmann, "Optimization of the OPLS-AA force field for long hydrocarbons," J. Chem. Theory Comput. **8**, 1459–1470 (2012).
[68]T. A. Halgren, "Merck molecular force field. II. MMFF94 van der Waals and electrostatic parameters for intermolecular interactions," J. Comput. Chem. **17**, 520–552 (1996).
[69]Y. Liang, M. Yang, W. Wu, X. Zhang, and J. Wang, "Experimental and kinetic modeling study of iso-dodecane: Pyrolysis and oxidation," J. Anal. Appl. Pyrolysis **188**, 106998 (2025).
[70]L. Xin, C. Liu, Y. Liu, E. Huo, Q. Li, X. Wang, and Q. Cheng, "Thermal decomposition mechanism of some hydrocarbons by REAXFF-based molecular dynamics and density functional theory study," Fuel **275**, 117885 (2020).
[71]J. H. Birely and J. L. Lyman, "The effect of reagent vibrational energy on measured reaction rate constants," J. Photochem. **4**, 269–280 (1975).
[72]L. Piela, *Ideas of Quantum Chemistry* (Elsevier, 2013).
[73]W. Zhang and A. C. T. van Duin, "Second-generation REAXFF water force field: Improvements in the description of water density and OH-anion diffusion," J. Phys. Chem. B **121**, 6021–6032 (2017).

06 May 2025 09:58:34

© Author(s) 2025